

# The non-resonant, relativistic dynamics of circumbinary planets

Cezary Migaszewski<sup>1\*</sup> and Krzysztof Goździewski<sup>1\*†</sup>

<sup>1</sup>Toruń Centre for Astronomy, Nicolaus Copernicus University, Gagarin Str. 11, 87-100 Toruń, Poland

Accepted .... Received ...; in original form ...

## ABSTRACT

We investigate the model of a hierarchical planetary system composed of point masses, taking into account relativistic corrections to the Newtonian gravity. We focus on the non-resonant system of a compact stellar (or sub-stellar) binary and a low-mass companion (a planet or a brown dwarf) in well separated and inclined orbit to the orbital plane of the binary (the circumbinary planet). The model relies on the expansion of the perturbing, averaged Hamiltonian in terms of the ratio of semi-major axes  $\alpha$ . We found that the low-mass object in a distant orbit may excite large eccentricity of the inner binary when the mutual inclination of the orbits is larger than about of 60 deg. This unusual behavior is related to strong instability caused by a dynamical phenomenon that is similar to the Lidov-Kozai resonance (LKR). The secular system may be strongly chaotic. Our study shows that in the Jupiter– or brown dwarf–mass regime of the low-massive companion, the restricted model does not properly describe the long-term dynamics in the vicinity of the LKR. The relativistic correction is significant for the parametric structure of a few families of stationary solutions in this problem, in particular, for the direct orbits configurations. We found that the dynamics of hierarchical systems with small  $\alpha \sim 0.01$  may be qualitatively different in the realm of the Newtonian (classic) and relativistic models. This holds true even for relatively large masses of the secondaries.

**Key words:** celestial mechanics – secular dynamics – analytical methods – stationary solutions – extrasolar planetary systems

## 1 INTRODUCTION

The extrasolar planets are discovered routinely<sup>1</sup>. Recently, about of 500 low-mass companions to stars of different spectral types are known. Most of them are bounded to single stars. Moreover, there is also a growing number of planetary candidates in binaries as well as multi-stellar systems (see Eggenberger 2010, for the statistical properties of planets in binaries). Generally, following nomenclature in (Rabl & Dvorak 1988), we can consider two classes of such multiple systems. In the *satellite case* or the S-type configuration, a planet revolves around one of the primaries in the binary, and the second primary is much more distant. In the *cometary or circumbinary* configuration (C-type from hereafter), the planet has a wide orbit around the inner, massive binary.

Current theories of planet formation in multiple stellar systems (e.g., Takeda et al. 2009, and references therein) show that the inclination of a planetary orbit to the orbital plane of the binary may be non-zero in the C-type and the S-type systems. It is well known that in the S-type configurations, when the mutual inclination of circular orbits is larger than the critical value  $i_{\text{crit}} \sim 40^\circ$ , the inner orbit undergoes large-amplitude oscillations of the eccen-

tricity, which is in anti-phase with the mutual inclination. This dynamical phenomenon is well known as the Kozai (or Lidov–Kozai) resonance (Lidov 1962; Kozai 1962). We will call it the LKR from hereafter. Keeping in mind the two types of possible orbital configurations, this instance of the LKR may be also understood as *the inner LKR* (see, e.g., Krasinskii 1972, 1974). Actually, many authors explain large eccentricities of some planetary candidates due to forcing by a distant star or massive companion (see, e.g., Tamuz 2008; Fabrycky & Tremaine 2007). In fact, the amplification of eccentricity and inclination may also appear in the C-type systems. The critical inclination is then  $\sim 60^\circ$ , and it may be attributed to *the outer LKR* (see, e.g., Krasinskii 1972, 1974; Migaszewski & Goździewski 2010), and this will be addressed further in this work.

In the literature, the problem is most often considered as the restricted one, which means that the planet is a mass-less particle not perturbing the motion of the binary. It has been studied in many papers, with different analytical and numerical techniques. The restricted model help us to simplify the analysis, nevertheless, the assumption of negligible influence of the planet on the motion of primaries may be not valid if the planet is large. In fact, low-mass objects in a few Jupiter-mass range are quite common. If the mutual interactions are significant, as we will show further in this work, the binary orbit may be strongly perturbed by a distant, relatively massive planet or a brown dwarf moving in inclined, wide orbit, even if the mass of inner companion is *ten times* larger than the perturber.

In this work, we focus on the unrestricted C-type problem by

\* E-mail: c.migaszewski@astri.uni.torun.pl

† E-mail: k.gozdziwski@astri.uni.torun.pl

<sup>1</sup> The recent detections and literature are frequently updated by Jean Schneider in [www.exoplanet.eu](http://www.exoplanet.eu)

means of the secular model in terms of the semi-major axes ratio,  $\alpha$ . We assume that  $\alpha$  is small ( $< 0.1$ ), hence we focus on hierarchical systems. In such a case, we face very different times scales of the orbital evolution. Typically, the inner binary has the orbital period counted in months or years but the period of the outer planet is at least  $\sim 100$  times longer. Hence the short-term mean motion resonances (MMRs) are not present in the system. The secular evolution of the mean orbits, depending on the mutual interactions, is even much longer, and spans Myr time-scale. To follow the orbital evolution in all these time-scales in details, one could integrate the equations of motion numerically. Unfortunately, this direct, brute-force approach requires too large CPU overhead.

Because we are primarily interested in the long-term evolution of the hierarchical systems, the problem may be simplified with the help of the averaging principle. The Hamiltonian of the hierarchical system may be splitted onto integrable Keplerian part of the inner binary, and for the perturbation part of the mutual interaction with the low-mass companion. Because the system is non-resonant, the perturbing Hamiltonian may be averaged out over the mean anomalies or the mean longitudes, which play the role of the fast angles. After the averaging, we obtain the secular Hamiltonian describing the long-term evolution of the mean, slowly varying orbits. To obtain the secular model, we extend a simple averaging scheme (the so called *mixed anomalies method*) in our earlier paper (Migaszewski & Goździewski 2008) to the non-coplanar case. The perturbing Hamiltonian is expanded with respect to  $\alpha$ , and then the series may be averaged out term by term. We derived such averaged expansion of the secular Hamiltonian to the 10-th order in  $\alpha$ . It is a more general version of the third-order (octupole-level) theory, studied in the planetary context in (Ford et al. 2000; Lee & Peale 2003) and of the integrable, second order (quadrupole-level) approximation in many papers (e.g., Harrington 1968; Krasinski 1972; Lidov & Ziglin 1976; Ferrer & Osácar 1994; Farago & Laskar 2010, and references therein).

Our work is closely related to remarkable study by Michtchenko et al. (2006), to which we will refer many times, as well as to our earlier paper (Migaszewski & Goździewski 2009a) devoted to the analysis of equilibria in the three-dimensional problem of two planets. Moreover, this work extends these papers in two important aspects. The averaging of the secular problem is done analytically, which simplifies and optimizes the computations, helping us to avoid numerical artifacts. Here, we also consider a generalization of the Newtonian model, by accounting for the leading non-Newtonian point-mass corrections to the perturbing Hamiltonian, i.e., the relativistic, post-Newtonian (PN) correction. It can be also easily averaged out over the mean anomalies. The PN corrections are particularly important if the frequencies of the slow angles which they induce, are comparable with the frequencies caused by the *Newtonian* interactions (e.g., Adams & Laughlin 2006; Fabrycky & Tremaine 2007). We shown already (Migaszewski & Goździewski 2009b) that accounting for the relativistic corrections in the co-planar case of two-planet system may lead to qualitatively different global view of the phase space in both models. Hence, the PN correction might be also important in the 3D problem. Indeed, as we will show below, this apparently subtle effect induces global, qualitative changes of the structure of the phase space.

A plan of this paper is as follows. In Sections 2 and 3, we derive the 3D secular model of the planetary system, in that the mean motion resonances of low order are absent, following the coplanar case considered in (Migaszewski & Goździewski 2008). We try to keep the presentation self-contained, therefore we recall basic

facts regarding the dynamics of the secular model, which might be found in other papers already published. Section 3 describes a test of the secular approximation, and recalls the notion of the so called representative planes of initial conditions, as well as a scheme of investigating families of stationary solutions in the secular model. Section 4 is for the analysis of the eccentricity evolution and chaotic dynamics. Section 5 is devoted to a parametric survey of the equilibria in the classic (point-mass Newtonian) model. In Sect. 6, we study influence of the PN corrections on these solutions. In Conclusions, we summarize the results and sketch perspectives of the further research.

## 2 THE SECULAR 3D MODEL OF $N$ -PLANETS

We consider the general, spatial model of the  $N$ -planet system around a central star. It may be described in terms of the Hamiltonian written with respect to canonical Poincaré variables (Michtchenko et al. 2006) in the form of  $\mathcal{H} = \mathcal{H}_{\text{kepl}} + \mathcal{H}_{\text{pert}}$ , where

$$\mathcal{H}_{\text{kepl}} = \sum_{i=1}^N \left( \frac{\mathbf{p}_i^2}{2\beta_i^*} - \frac{\mu_i^* \beta_i^*}{r_i} \right), \quad (1)$$

stands for the integrable part comprising of the direct sum of the relative, Keplerian motions of point-mass secondaries  $m_i$ ,  $i = 1, \dots, N$ , with respect to the primary mass  $m_0$ . We also define the mass parameters  $\mu_i^* = k^2 (m_0 + m_i)$ , where  $k$  is the Gauss gravitational constant, and  $\beta_i^* = (1/m_i + 1/m_0)^{-1}$  are the so called reduced masses. The term  $\mathcal{H}_{\text{pert}}$  stands for the perturbing function of the Keplerian motions. We assume that the perturbation is a sum of two terms:

$$\mathcal{H}_{\text{pert}} = \mathcal{H}_{\text{NG}} + \mathcal{H}_{\text{GR}}, \quad (2)$$

where  $\mathcal{H}_{\text{NG}}$  is related to a *small* Newtonian mutual interactions between  $m_i$  and  $m_j$ , and we assume that  $\mathcal{H}_{\text{pert}}/\mathcal{H}_{\text{kepl}} \ll 1$ . That may be accomplished either by keeping  $m_i$  small (then we have the *planetary regime*) or permitting that secondary masses are relatively large (even comparable with the central object) and simultaneously requiring large separations between particular orbits (the *stellar regime*). The term of  $\mathcal{H}_{\text{GR}}$  is for the leading general relativity (PN) corrections to the potential of the central star and the innermost companion. Here we focus on the non-resonant systems, with well separated orbits, hence we may neglect the relativistic post-Newtonian perturbations of the outer bodies. If the semi-major axes ratios  $\alpha_{i,j} = a_i/a_j < 0.1$  are small, the relativistic corrections for the distant objects are by orders of magnitude smaller than the PN perturbation of the inner binary.

Following the notion of the Poincaré coordinates, the  $\mathcal{H}_{\text{NG}}$  perturbation may be written as follows:

$$\mathcal{H}_{\text{NG}} = \sum_{i=1}^{N-1} \sum_{j>i}^N \left( \underbrace{-\frac{k^2 m_i m_j}{\Delta_{i,j}}}_{\text{direct part}} + \underbrace{\frac{\mathbf{p}_i \cdot \mathbf{p}_j}{m_0}}_{\text{indirect part}} \right), \quad (3)$$

where  $\mathbf{r}_i$ ,  $i = 1, \dots, N$  are for the position vectors of  $m_i$  relative to the central body,  $\mathbf{p}_i$  are for their conjugate momenta relative to the *barycenter* of the whole  $(N+1)$ -body system,  $\Delta_{i,j} = \|\mathbf{r}_i - \mathbf{r}_j\|$  denote the relative distance between bodies  $i$  and  $j$ .

After (Richardson & Kelly 1988), or developing the PN Hamiltonian from the general Lagrangian in (Brumberg 2007), the post-Newtonian potential in the PN formulation,  $\mathcal{H}_{\text{GR}} \equiv \beta^* \mathcal{H}'_{\text{GR}}$ , where  $\mathcal{H}'_{\text{GR}}$  has the following form:

$$\mathcal{H}'_{\text{GR}} = \gamma_1 \mathbf{P}^4 + \gamma_2 \frac{\mathbf{P}^2}{r} + \gamma_3 \frac{(\mathbf{r} \cdot \mathbf{P})^2}{r^3} + \gamma_4 \frac{1}{r^2}, \quad (4)$$

with coefficients  $\gamma_1, \gamma_2, \gamma_3, \gamma_4$ :

$$\gamma_1 = -\frac{(1-3\nu)}{8c^2}, \quad \gamma_2 = -\frac{\mu^*(3+\nu)}{2c^2}, \quad \gamma_3 = \frac{(\mu^*)^2}{2c^2}, \quad \gamma_4 = -\frac{\mu^*\nu}{2c^2},$$

where  $c$  stands for the speed of light in a vacuum,  $\mu^* = k^2(m_0 + m_1)$ ,  $\nu \equiv m_0 m_1 / (m_0 + m_1)^2$ ,  $\mathbf{P}$  is the astrometric momentum of the innermost secondary (normalized through the reduced mass):

$$\mathbf{P} = \mathbf{v} + \frac{1}{c^2} \left[ 4\gamma_1 (\mathbf{v} \cdot \mathbf{v}) \mathbf{v} + \frac{2\gamma_2}{r} \mathbf{v} + \frac{2\gamma_4}{r^3} (\mathbf{r} \cdot \mathbf{v}) \mathbf{r} \right], \quad (5)$$

and  $\mathbf{v} \equiv \dot{\mathbf{r}}$  stands for the astrometric velocity of the innermost object (still, assuming that the relativistic corrections from the other bodies in the system are neglected). Hence,  $\mathbf{P} = \mathbf{v}$  with the accuracy of  $\mathcal{O}(c^{-2})$  and then the relativistic Hamiltonian is conserved up to the order of  $\mathcal{O}(c^{-4})$ .

It is well known that the equations of motion of the  $N$ -body system with  $N \geq 3$  are not integrable. However, making use of the assumptions above, we may apply the averaging proposition (Arnold et al. 1993) to remove the short order perturbations, and to derive the equations of the secular dynamics, governing the long-term evolution of the *mean* orbital elements.

To perform the averaging, the perturbation must be expressed in terms of the canonical action-angle variables  $(\mathbf{I}, \phi)$ :

$$\mathcal{H}(\mathbf{I}, \phi) = \mathcal{H}_{\text{kepl}}(\mathbf{I}) + \mathcal{H}_{\text{pert}}(\mathbf{I}, \phi), \quad (6)$$

and we assume that  $\mathcal{H}_{\text{pert}}(\mathbf{I}, \phi) \sim \varepsilon \mathcal{H}_{\text{kepl}}(\mathbf{I})$ , where  $\varepsilon \ll 1$  is a small parameter. Here, we use the mass-weighted Delaunay elements (e.g., Murray & Dermott 2000):

$$\begin{aligned} l_i &\equiv \mathcal{M}_i, & L_i &\equiv \beta_i^* \sqrt{\mu_i^*} a_i, \\ g_i &\equiv \omega_i, & G_i &\equiv L_i \sqrt{1 - e_i^2}, \\ h_i &\equiv \Omega_i, & H_i &\equiv G_i \cos I_i, \end{aligned} \quad (7)$$

where  $\mathcal{M}_i$  are the mean anomalies,  $a_i$  stand for canonical semi-major axes,  $e_i$  are the eccentricities,  $I_i$  denote inclinations,  $\omega_i$  are the arguments of pericenter, and  $\Omega_i$  denote the longitudes of ascending node. The Hamiltonian of the  $N$ -planet system written in terms of these Delaunay variables (Eq. 7) has the form of:

$$\mathcal{H} = - \sum_{i=1}^N \frac{(\mu_i^*)^2 (\beta_i^*)^3}{2L_i^2} + \mathcal{H}_{\text{pert}}(\underbrace{L_i, l_i, G_i, g_i, H_i, h_i}_{i=1, \dots, N}). \quad (8)$$

In this formulation,  $l_i$  are the fast angles. They may be eliminated through the averaging that is accomplished with:

$$\mathcal{H}_{\text{sec}} = \frac{1}{(2\pi)^N} \int_0^{2\pi} \dots \int_0^{2\pi} \mathcal{H}_{\text{pert}} d\mathcal{M}_1 \dots d\mathcal{M}_N. \quad (9)$$

We should remember here that  $\mathcal{H}_{\text{sec}}$  is valid only if (1)  $\mathcal{H}_{\text{pert}} \sim \varepsilon \mathcal{H}_{\text{kepl}}$  (where  $\varepsilon \ll 1$  means a small parameter), and the averaging of the *unperturbed* Keplerian orbits is equivalent to performing the first step in terms of the perturbation calculus (Ferraz-Mello 2007), (2) there is no mixed resonances between the inner binary and the outer companion (e.g., between slow frequencies of the inner orbit and the mean motion of the outer orbit). We checked, that planetary systems studied in this paper, within the respective parameter ranges, obey these assumptions.

Because the secular Hamiltonian  $\mathcal{H}_{\text{sec}}$  does not depend on mean anomalies  $\mathcal{M}_i$ , the conjugate momenta  $L_i$  are integrals of the secular problem. Obviously, the mean semi-major axes are also constant, hence we get rid of  $N$ -degrees of freedom (DOF).

### 3 AVERAGING THE 3D MODEL OF $N$ -PLANETS

In (Migaszewski & Goździewski 2008), we describe a simple scheme of the averaging the perturbing function  $\mathcal{H}_{\text{pert}}$  (Eq. 2) in coplanar case, which makes use of the very basic properties of the Keplerian motion, the mixed anomalies algorithm. This method may be easily applied to the 3D problem. At first, we consider the *direct* part of the mutual interaction between the planets,  $\mathcal{H}_{\text{NG}}$  (Eq. 3). The *indirect* part averages out to a constant and does not contribute to the secular dynamics (Brouwer & Clemence 1961).

The secular Hamiltonian may be written as a sum of terms representing mutual interactions between all pairs of planets  $i < j$ , where  $a_i < a_j$ :

$$\langle \mathcal{H}_{\text{NG}} \rangle = \sum_{i=1}^{N-1} \sum_{j>i}^N \langle \mathcal{H}_{\text{NG}}^{(i,j)} \rangle. \quad (10)$$

For a particular pair of planets, we calculate the following integral:

$$\langle \mathcal{H}_{\text{NG}}^{(i,j)} \rangle = \frac{1}{(2\pi)^2} \int_0^{2\pi} \int_0^{2\pi} -\frac{k^2 m_i m_j}{\Delta_{i,j}} d\mathcal{M}_i d\mathcal{M}_j. \quad (11)$$

Hence, the problem may be reduced to averaging the inverse of the distance  $\Delta_{i,j}$  between two particular planets over their mean anomalies:

$$\Delta_{i,j} = \sqrt{r_i^2 + r_j^2 - 2\mathbf{r}_i \cdot \mathbf{r}_j}, \quad (12)$$

where  $\mathbf{r}_i$  and  $\mathbf{r}_j$  must be expressed in a common reference frame  $\mathcal{F}$ . The same vectors, written in the orbital reference frames  $\mathcal{F}_i$  of each planet, are  $\mathbf{r}_i|_{\mathcal{F}_i} = [x_i, y_i, 0]^T$ , and expressed in the common reference frame, they have the form of:  $\mathbf{r}_i = \mathbb{A}_i \mathbf{r}_i|_{\mathcal{F}_i}$ . Here, the rotation matrix  $\mathbb{A}_i \equiv \mathbb{A}_i(\omega_i, \Omega_i, I_i)$  is the matrix product of elementary Eulerian rotations (Murray & Dermott 2000):

$$\mathbb{A}_i(\omega_i, \Omega_i, I_i) = \mathbb{P}_3(-\Omega_i) \mathbb{P}_1(-I_i) \mathbb{P}_3(-\omega_i).$$

Formulae 12 may be rewritten as follows:

$$\Delta_{i,j} = r_j \sqrt{1 - 2 \frac{1}{r_j} \mathbf{r}_i \cdot \frac{\mathbf{r}_j}{r_j} + \left( \frac{r_i}{r_j} \right)^2}. \quad (13)$$

Following (Migaszewski & Goździewski 2008), we express the radius vector  $\mathbf{r}_i$  of the inner body in each planetary pair with respect to the eccentric anomaly. The radius vector of the outer body in the pair is parametrised by the true anomaly. This choice implies that  $\Delta_{i,j}^{-1}$  expanded in Taylor series with respect to  $\alpha$  is a trigonometric polynomial. To compute the integral in Eq. 11, we also change the integration variables:

$$d\mathcal{M}_i \equiv I_i dE_i, \text{ and } d\mathcal{M}_j \equiv \mathcal{J}_j df_j,$$

where auxiliary functions appear:

$$I_i = 1 - e_i \cos E_i, \quad \mathcal{J}_j = \frac{(1 - e_j)^{3/2}}{(1 + e_j \cos f_j)^2}. \quad (14)$$

Finally, the averaged mutual perturbation has the same general form as in the coplanar case (Migaszewski & Goździewski 2008):

$$\begin{aligned} \langle \mathcal{H}_{\text{NG}}^{(i,j)} \rangle &= -\frac{k^2 m_i m_j}{a_j} \times \\ &\times \left[ 1 + \sqrt{1 - e_j^2} \sum_{l=2}^{\infty} \mathcal{X}_{i,j}^l \mathcal{R}_l^{(i,j)}(e_i, e_j, \omega_i, \omega_j, \Omega_i, \Omega_j, I_i, I_j) \right], \end{aligned} \quad (15)$$

although explicit expressions for  $\mathcal{R}_l^{(i,j)}$  are obviously different in the 3D model. The zeroth-order term in Eq. 15 is reduced to a

constant and does not influence the secular equations of motion. Also the first order term vanishes identically. The remaining terms  $\mathcal{R}_l^{(i,j)}$  have rather complex form. In the simplest three-body system ( $i \equiv 1, j \equiv 2$ ), we may express them in the Laplace reference frame. In this case,  $\Delta\Omega = \pm\pi$  and  $G_1 \sin I_1 = G_2 \sin I_2$  (see e.g., Michtchenko et al. 2006). It is also natural to introduce the mutual inclination,  $i_{\text{mut}} \equiv I_1 + I_2$ . Then the  $\mathcal{R}_l^{(i,j)}$ -terms of the order of 2 and 3 may be identified with the *quadrupole* and *octupole* terms, respectively (see, e.g., Ford et al. 2000; Lee & Peale 2003; Farago & Laskar 2010). The quadrupole-level term is the following:

$$\mathcal{R}_2^{(1,2)} = \frac{1}{8}D_1 \left(2 + 3e_1^2\right) - \frac{15}{16}e_1^2 D_2 \cos 2\omega_1, \quad (16)$$

where  $C_l \equiv \cos i_{\text{mut}}$ , and  $D_1 = (3C_l^2 - 1)/2$ ,  $D_2 = C_l^2 - 1$ . The third order (octupole-level) term reads as follows:

$$\begin{aligned} \mathcal{R}_3^{(1,2)} = & -\frac{15}{64}D_6 e_1 e_2 \cos \Delta\omega \left(3e_1^2 + 4\right) \\ & -\frac{525}{256}D_3 D_2 e_1^3 e_2 \cos(3\omega_1 - \omega_2) \\ & -\frac{525}{512}D_4 D_2 e_1^3 e_2 \cos(3\omega_1 + \omega_2) \\ & +\frac{15}{128}D_5 e_1 e_2 \cos(\omega_1 + \omega_2) \\ & +\frac{45}{512}D_5 e_1^3 e_2 \cos(\omega_1 + \omega_2), \end{aligned} \quad (17)$$

where coefficients  $D_j$  are:

$$\begin{aligned} D_3 &= (1 + C_l)/2, \quad D_4 = 1 - C_l, \\ D_5 &= -15C_l^3 + 5C_l^2 + 11C_l - 1, \\ D_6 &= (15C_l^3 + 5C_l^2 - 11C_l - 1)/8. \end{aligned}$$

Equations 16 and 17 are written similarly to terms appearing in the coplanar model [see equations (22) and (23) in (Migaszewski & Goździewski 2008)]. Clearly, if  $i_{\text{mut}} = 0$  then  $D_1 = D_3 = D_6 = 1$ ,  $D_2 = D_4 = D_5 = 0$ , and formulae  $\mathcal{R}_2^{(i,j)}$ ,  $\mathcal{R}_3^{(i,j)}$  coincide with those ones of in the coplanar problem.

An explicit expansion of  $\mathcal{H}_{\text{sec}}$  shows that the quadrupole-order term in  $\alpha$  introduces the evolution of eccentricity  $e_1$ , and in this approximation, the outer eccentric  $e_2$  is constant. The variation of the outer eccentricity may be only introduced through the third order (octupole) and higher terms. Indeed, up to the quadrupole approximation, the secular Hamiltonian does not depend on  $\omega_2$  (the cyclic angle), and the eccentricity of the outer body becomes an additional integral of motion. In this case, the problem can be reduced to one DOF and is integrable (Lidov & Ziglin 1976). This feature has been accounted for in many recent papers, moreover, the apparently subtle third-order perturbation to the Keplerian model, or the first order perturbation to the integrable quadrupole-order approximation may introduce qualitative changes of the dynamics.

We calculated the secular expansion (Eq. 15) up to the 10-th order<sup>2</sup>. One should be aware that by increasing the order of this expansion, we do not necessarily improve the approximation of the secular model of the real system, because this model is still limited by the first order perturbation theory. In Section 3.2 we will examine the accuracy of the secular expansion in more details.

Finally, the averaged relativistic correction possesses the same form as in coplanar case (Migaszewski & Goździewski 2008).

Moreover, we include this perturbation only to the mutual interaction of masses  $m_0$  and  $m_1$ :

$$\langle \mathcal{H}_{\text{GR}} \rangle = -\frac{3(\mu_1^*)^4 (\beta_1^*)^5}{c^2 L_1^3 G_1} + \text{const}, \quad (18)$$

as it was explained above.

### 3.1 A global, 2-dim representation of the phase space

Because the general planetary  $N$ -body problem is very complex, we restrict the further analysis to its simplest, non-trivial case of three bodies. We shall consider configurations of the host star and two planets or C-type systems comprising of a binary and a more distant body (a planet).

We recall that the secular Hamiltonian  $\mathcal{H}_{\text{sec}}$  of the three body problem does not depend on  $\mathcal{M}_1, \mathcal{M}_2$ , therefore the conjugate actions  $(L_1, L_2)$  are constant. The Hamiltonian  $\mathcal{H}$  written in the Laplace reference frame depends on  $\Delta\Omega = \Omega_2 - \Omega_1 \equiv \pm\pi$  only, not on  $\Omega_1$  and  $\Omega_2$  separately. Hence, the following canonical transformation (e.g., Michtchenko et al. 2006):

$$\begin{aligned} (\omega_1, G_1) & \rightarrow (\omega_1, G_1) \\ (\omega_2, G_2) & \rightarrow (\omega_2, G_2) \\ (\Omega_1, H_1) & \Rightarrow \left( \theta_1 = \frac{1}{2}(\Omega_1 + \Omega_2), J_1 = H_1 + H_2 \right) \\ (\Omega_2, H_2) & \Rightarrow \left( \theta_2 = \frac{1}{2}(\Omega_1 - \Omega_2), J_2 = H_1 - H_2 \right) \end{aligned} \quad (19)$$

removes  $\Omega_1, \Omega_2$  from the secular Hamiltonian. After this transformation it does not depend on  $\theta_1$ , therefore  $J_1 \equiv |\mathbf{C}| = C = \text{const}$ , where  $\mathbf{C}$  is the total angular momentum of the system. Moreover,  $\theta_2 = \pm\pi/2 = \text{const}$  (after the Jacobi reduction of nodes) and  $J_2$  may be expressed as a function of  $G_1, G_2$  and  $J_1$  in the following form:

$$J_2 = (G_1^2 - G_2^2)/J_1.$$

Therefore, for constant values of the angular momentum  $J_1 \equiv C$  and the secular energy  $\mathcal{H}_{\text{sec}}$ , the secular dynamics are reduced to two DOF Hamiltonian system. Instead of the total angular momentum  $C$ , we shall use the so called Angular Momentum Deficit (AMD) (Laskar 2000):

$$\text{AMD} = L_1 + L_2 - C,$$

or its *normalized* value of  $\mathcal{A} \equiv \text{AMD}/(L_1 + L_2)$ ,  $\mathcal{A} \in [0, 1]$  (Migaszewski & Goździewski 2009a). Because  $L_1, L_2$  and  $C$  are integrals of the secular system, the relativistic correction, Eq. 18 does not change  $\mathcal{A}$ , and the DOF number does not change. Because  $\langle \mathcal{H}_{\text{GR}} \rangle$  depends on  $G_1$  only, thus it affects only the temporal evolution of  $\omega_1$ . We note here that the perturbation induced by the quadrupole moment of the star, which was discussed (Migaszewski & Goździewski 2009b) in the coplanar case, also depends on  $H_1$  in the 3D problem, i.e. on the orbital inclination to the equatorial plane of the star. This perturbation introduces an additional frequency to  $\Omega_1$  and then  $\Delta\Omega$  is not constant anymore. It means that we could not perform the reduction of nodes and the secular problem would have three DOF. This also means that the Laplace reference frame, defined in terms of the total orbital angular momentum, does not possess any constant orientation in space. Being aware of this problem, we do not consider the dynamical flattening of the star and/or of the innermost planet. The two DOF model is then less general but the dynamics are better tractable, thanks to the geometrical tools, which can be applied to study this basic, low-dimensional problem.

If we fix the secular Hamiltonian in the form of  $\mathcal{H}_{\text{sec}} \equiv$

<sup>2</sup> This expansion is available on request in the form of a raw MATHEMATICA input file; it may be also available on-line, after publishing this manuscript.

$\mathcal{H}_{\text{sec}}(G_1, G_2, \omega_1, \omega_2)$ , then  $\mathcal{A}$  may be considered as a free parameter of the secular model. Moreover, the phase space is *four-dimensional*, and to represent the phase space of the system globally in terms of two-dimensional sections, which are easy to visualize, we follow a concept of *the representative plane of initial conditions* (Michtchenko & Malhotra 2004), the  $\Sigma$ -plane from hereafter. The  $\Sigma$ -plane may be chosen in different ways, although all representations may be fixed and defined through the following conditions:

$$\frac{\partial \mathcal{H}_{\text{sec}}}{\partial \omega_1} = 0, \quad \frac{\partial \mathcal{H}_{\text{sec}}}{\partial \omega_2} = 0. \quad (20)$$

These conditions imply that all phase trajectories of the secular system cross the  $\Sigma$ -plane (Michtchenko et al. 2006; Libert & Henrard 2007), see also our explanation in (Migaszewski & Goździewski 2009a). In accord with the symmetries in the secular 3D model, the solutions to these equations are the following four pairs of angles:

$$(\omega_1, \omega_2) = \{(0, 0); (0, \pm\pi); (\pm\pi/2, \pm\pi/2); (\pm\pi/2, \mp\pi/2)\}, \quad (21)$$

that also define four distinct quarters of the  $\Sigma$ -plane, numbered with Roman numbers II, I, IV, and III, respectively, see (Michtchenko et al. 2006) for details. In this sense, the  $\Sigma$ -plane may be thought as an analogue of the Poincaré cross section. The conditions fixing the characteristic plane may be also rewritten as follows:

$$\cos \omega_1 = \cos \omega_2 = 0 \cup \sin \omega_1 = \sin \omega_2 = 0.$$

Further, we shall use three, basically equivalent geometric representations of the  $\Sigma$ -plane, which cover certain combinations of the quarters (the solution pairs of the pericenter arguments):

- the  $\mathcal{P}_S$ -plane is defined with  $\cos \omega_1 = \cos \omega_2 = 0$ , and

$$\mathcal{P}_S = \{x = e_1 \sin \omega_1, y = e_2 \sin \omega_2, e_1 \in [0, 1], e_2 \in [0, 1]\}, \quad (22)$$

- the  $\mathcal{P}_C$ -plane is defined with  $\sin \omega_1 = \sin \omega_2 = 0$ , and

$$\mathcal{P}_C = \{x = e_1 \cos \omega_1, y = e_2 \cos \omega_2, e_1 \in [0, 1], e_2 \in [0, 1]\}, \quad (23)$$

- and, finally, two incarnations of the  $\mathcal{S}$ -plane:

$$\mathcal{S} = \{x = e_1 \cos \Delta \varpi, y = e_2 \cos 2\omega_1, e_1 \in [0, 1], e_2 \in [0, 1]\}, \quad (24)$$

$$\mathcal{S}' = \{x = e_1 \cos 2\omega_1, y = e_2 \cos \Delta \varpi, e_1 \in [0, 1], e_2 \in [0, 1]\}, \quad (25)$$

that was defined originally in (Michtchenko et al. 2006). It can be shown, that the  $\mathcal{P}_S$ - and  $\mathcal{P}_C$ -planes carry out the same information as the  $\mathcal{S}$ -plane. However, the  $\mathcal{S}$ -plane has a discontinuity along the  $x$ -axis, and the former representations are sometimes more convenient to the analysis of solutions of the secular system.

### 3.2 A test of the analytic model

We left a test of the accuracy of the secular expansion to this end, because the introduced  $\Sigma$ -planes are useful to illustrate the results of this test in a global manner. We select initial conditions in the  $\mathcal{S}$ -plane, and the secular energy computed with the help of the analytic expansion is compared with the results of numerical averaging developed in (Gronchi & Milani 1998; Michtchenko & Malhotra 2004), which are exact up to the numerical quadrature error. We consider the non-relativistic case only, because the secular relativistic correction is exact (with the first non-zero post-Newtonian term included), and it does not influence the precision of analytic formulae. Figure 1 shows the levels of  $\mathcal{H}_{\text{sec}}$ , marked with solid curves in the  $\mathcal{S}$ -plane. Each panel is for a different order of the analytic approximation. The relative difference between values of

the mean Hamiltonians, derived through the analytic (“A”) and numerical (“N”) algorithms may be defined as follows:

$$\Delta_l \equiv \left\| \frac{\mathcal{H}_{\text{sec}}^A(l) - \mathcal{H}_{\text{sec}}^N}{\mathcal{H}_{\text{sec}}^N} \right\|, \quad (26)$$

where  $l$  is the order of the analytic expansion in  $\alpha$ . The results of this comparison are illustrated in Fig. 1 that shows the levels of  $\Delta_l$  computed for a hierarchical system with  $\alpha = 0.04$  and  $\mu \equiv m_1/m_2 = 5$ . The quadrupole-level model reproduces the secular Hamiltonian as the even function with respect to both  $x \equiv e_1 \{\sin, \cos\} \omega_1$  and  $y \equiv e_2 \{\sin, \cos\} \omega_2$ . The higher order approximations of  $\mathcal{H}_{\text{sec}}$  broke this symmetry. We have shown in (Migaszewski & Goździewski 2009a) that the shape of  $\mathcal{H}_{\text{sec}}$  significantly depends on  $\alpha$ . This is more important in the spatial problem, because even for relatively small  $\alpha$ , the quadrupole model distorts the structure of the phase-space (see Sect. 4.1). An inspection of Fig. 1 reveals that the octupole model reconstructs the secular Hamiltonian and its shape in the  $\mathcal{S}$ -plane very well, because the largest deviations  $\Delta_3 \sim 10^{-3}$  appear only for  $e_1 \sim 1$ . In other parts of the representative plane,  $\Delta_3 \sim 10^{-5}$ . The high-order expansions are obviously even more precise.

The octupole model introduces the first order perturbation to the integrable quadrupole model, hence, because it is very precise in the range of small  $\alpha$ , we further focus on this most simple, non-trivial case.

### 3.3 Equilibria in the secular 3D problem

In this work, we focus on the simplest class of solutions that are the equilibria (or stationary solutions). These solutions imply the basic structure of the phase space. By determining their stability, we may derive the local structure of neighboring phase trajectories through relatively simple analysis. The equilibria of the non-resonant system in terms of the quadrupole approximations were studied in the past, (e.g., Krasinski 1974; Lidov & Ziglin 1976). In our earlier work (Migaszewski & Goździewski 2009a), we classified families of equilibria emerging in the two-planet, non-planar problem, in terms of the quasi-analytic averaging, and basically exact secular model. We studied a few families of equilibria known in the literature, e.g., the zero-eccentricity solutions and the Lidov-Kozai resonance. We also found new families of these equilibria, in particular, the so called *chained orbits* solution that could be hardly derived with the perturbative approach, although the results in Gronchi & Milani (1998) might be applied here. This work focus on the planetary regime of parameters  $\mu, \alpha$ , the mass ratio  $\mu$  was restricted to the range of  $[0.1, 2]$  and  $\alpha \in [0.1, 0.667]$ . Moreover, we explored the whole permitted range of  $\mathcal{A} \in [0, 1]$ . Yet we learned that the semi-analytic approach has serious disadvantages. All calculations, including the integrations of the equations of motions, and the stability analysis must be performed with the help of numerical algorithms. This may introduce large errors and hinders the analytic, qualitative analysis of the problem.

In this section, we extend the study of stationary solutions in (Migaszewski & Goździewski 2009a) to a wider range of the mass ratio,  $\mu > 2$ . Simultaneously, we consider smaller  $\alpha < 0.1$ . That makes it possible to apply the analytic model described and tested in Sect. 3. Because planets emerge most likely from remnants of a thin protoplanetary disk, we also restrict our attention to mutual inclinations up to  $i_{\text{mut}} \sim 90^\circ$  (direct orbits). In that range, we may find families of equilibria related to the zero-eccentricity orbits, and the LK resonance classified in (Migaszewski & Goździewski 2009a) as solutions of family IVa, accompanied by families IIIa, IIIb, and

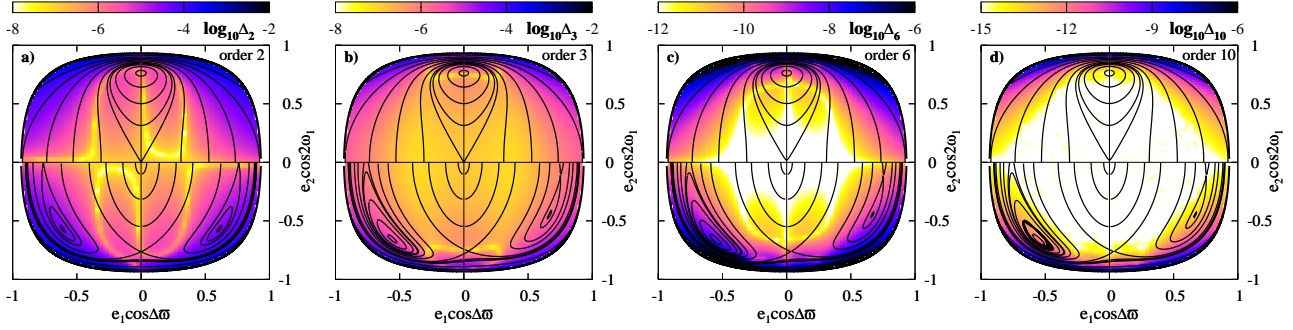


**Figure 1.** The precision of the analytic theory in terms of  $\Delta_l$ , Eq. 26, which is color-coded in the  $\mathcal{S}$ -plane. Parameters of the planetary system are as follows:  $\alpha = 0.04, \mu = 5, \mathcal{A} = 0.32$ . Panels from (a) to (d) are for the expansions in  $\alpha$  of the second, third, sixth, and tenth order, respectively.

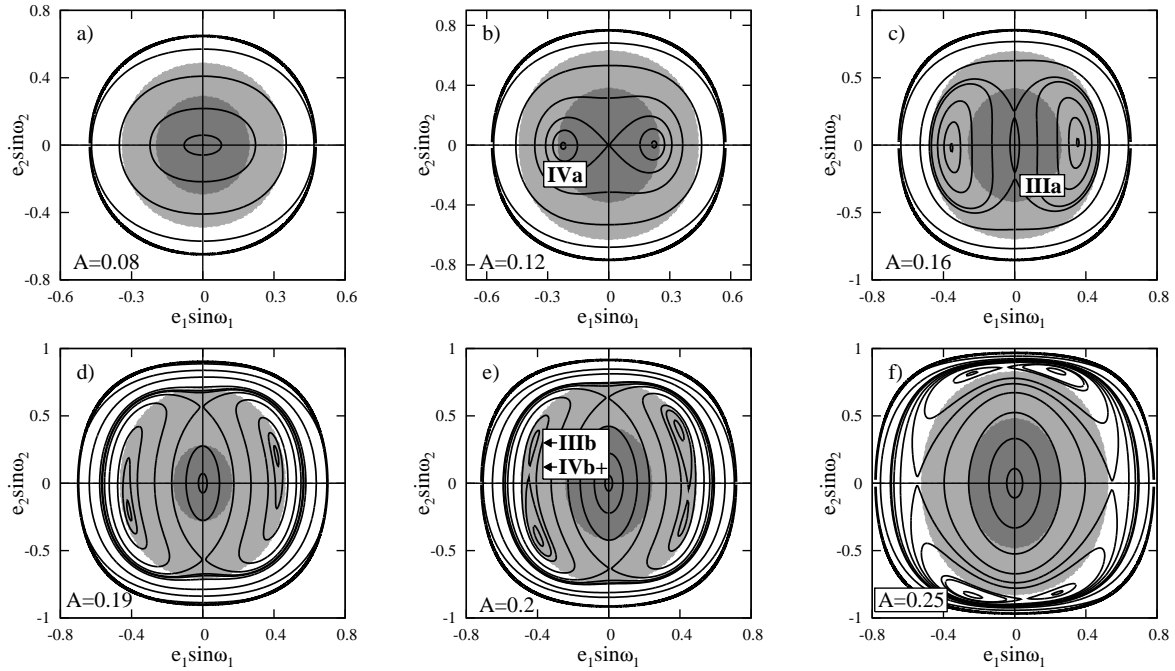


**Figure 2.** Levels of  $\mathcal{H}_{\text{sec}}$  at the  $\mathcal{P}_S$ -plane calculated for  $\alpha = 0.01$  and  $\mu = 20$ . Panels from a) to f) are for different values of  $\mathcal{A} = \{0.08, 0.12, 0.16, 0.19, 0.2, 0.25\}$ , respectively. These values of  $\mathcal{A}$  imply the mutual inclination at the origin  $i_0 = \{49^\circ, 61^\circ, 70^\circ, 77^\circ, 79^\circ, 89^\circ\}$ , respectively. The intensity of shaded areas encodes the mutual inclination in prescribed ranges, darker shade is for larger  $i_{\text{mut}}$ . The inclinations ranges are  $i_{\text{mut}} = (35^\circ, 45^\circ), (40^\circ, 55^\circ), (50^\circ, 65^\circ), (60^\circ, 75^\circ), (60^\circ, 75^\circ), (70^\circ, 85^\circ)$  in subsequent panels.

IVb+. Our analysis is also restricted to the initial conditions in quarters III and IV of the  $\mathcal{S}$ -plane, in which these solutions may only “reside”. This region of the parameter space has been studied (e.g., Krasinskii 1974) with the next-to-trivial quadrupole-level model. However, as we show below, this approximation may introduce artifacts due to the “non-real” symmetry of the secular Hamiltonian. Obviously, to avoid this problem, higher order expansions are required. We also attempt to extend the results of Ford et al. (2000), who applied the octupole-level theory to the analysis of hierarchical planetary systems with very small  $\alpha \sim 0.01$ .

To show the generic properties of the relevant families of equilibria, we begin with an example that is illustrated in Figure 2. Panels in this figure show levels of  $\mathcal{H}_{\text{sec}}$  at the  $\mathcal{P}_S$ -plane for  $\alpha = 0.01$  and  $\mu = 20$  and a few different values of  $\mathcal{A}$ . Panel 2a was derived for  $\mathcal{A} = 0.08$ , and it reveals the zero-eccentricity equilibrium. For larger  $\mathcal{A} = 0.12$  (Fig. 2b) the figure-eight structure of Lidov–Kozai equilibrium appears, and is labeled with IVa. We recall, that the

mutual inclination of circular orbits that corresponds to the LK bifurcation will be called the *critical inclination*,  $i_{\text{crit}}$  although, in general, any such value of the mutual inclination that leads to a bifurcation of equilibria has the sense of being “critical” (Krasinskii 1972, 1974). For larger value of  $\mathcal{A} = 0.16$  (Fig. 2c) the LKR “moves” towards larger  $e_1$  (simultaneously,  $e_2 \sim 0$ ) and a new saddle point appears. We call this solution a member of family IIIa. For larger  $\mathcal{A} = 0.19$  (Fig. 2d), these structures still expand, and for  $\mathcal{A} = 0.2$  (Fig. 2e) two new equilibria emerge: one is associated with quasi-elliptic point (family IIIb from hereafter), and a saddle of family IVb+. Apparently, it emerges from a point near the IVa solution in the  $\mathcal{P}_S$ -plane, nevertheless it does *not* correspond to a bifurcation of this equilibrium, see (Migaszewski & Goździewski 2009a). Solution IVa moves towards larger  $e_2$ , see Fig. 2f).

The *parametric paths* of these equilibria in terms of  $\mathcal{A}$ , may be depicted in the  $\mathcal{P}_S$ -plane (Fig. 3). Black and grey curves are for the stable and unstable equilibria, respectively. The relevant fami-

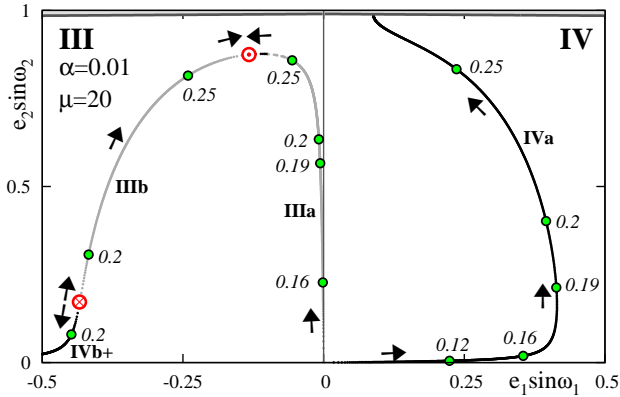


**Figure 3.** Families of stationary solutions (IVa, IIIa, IIIb, IVb+). Semi-major axes ratio  $\alpha = 0.01$ , mass ratio  $\mu = 20$ . Dark dots are for stable equilibria, grey dots are for unstable equilibria. Crossed and dotted circles mark bifurcations. Small arrows show the direction of particular stationary solution with increasing  $\mathcal{A}$ . Green dots are for the positions of equilibria for particular values of  $\mathcal{A} = 0.12, 0.16, 0.19, 0.2, 0.25$  (the energy levels are shown in Fig. 2). Solutions are for classic model, and were obtained with the help of the octupole theory.

lies of equilibria are labeled with Roman numbers and Latin letters. The direction of “motion” of particular solutions along the  $\mathcal{A}$ -axis is marked with arrows. For a reference, positions of the equilibria for a few discrete values of  $\mathcal{A} = 0.12, 0.16, 0.19, 0.2, 0.25$  (corresponding to subsequent panels in Fig. 2), are marked with green dots and labeled. Following a particular evolution path of equilibrium IVa, we see that it appears for  $\mathcal{A} \sim 0.1$  through a bifurcation of the origin. When  $\mathcal{A}$  increases, this solution moves along  $e_2 \sim 0$  towards larger  $e_1$ . For  $\mathcal{A} \sim 0.17$ , it reaches the maximal  $e_1 \sim 0.4$ , and it turns back, towards smaller  $e_1$  with simultaneous increase of  $e_2$ . When  $\mathcal{A}$  increases even more, this solution reaches the border of convergence of the analytic expansion. We call that border the *anti-collision line* [see (Migaszewski & Goździewski 2008)].

The parametric evolution of equilibria in quadrant III is more complex. The first non-trivial stationary solution appears for  $\mathcal{A} \sim 0.15$ , which is unstable, saddle point IIIa. It evolves along  $e_1 \sim 0$  and then  $e_2$  increases to large values. For  $\mathcal{A} \sim 0.195$ , two new solutions IIIb and IVb+ emerge from the elliptic structure related to the LKR (see Fig. 2e). One of them is stable (solution IVb+) and the another one is unstable (solution IIIb). They appear around  $(e_1 \sim 0.45, e_2 \sim 0.15)$ . When  $\mathcal{A}$  increases, the solution IVb+ moves towards  $e_1 \rightarrow 1$  and  $e_2 \rightarrow 0$ . Simultaneously, equilibrium IIIb is shifted towards increasing  $e_2$  and decreasing  $e_1$ . Then also IIIa increases  $e_2$  and leaves off the  $e_1 = 0$  axis. Finally, for  $\mathcal{A} \sim 0.26$ , equilibria IIIa and IIIb merge at one point  $(e_1 \sim 0.13, e_2 \sim 0.8)$ .

#### 4 THE SECULAR CHAOS

Following (Michtchenko et al. 2006), we shown in (Migaszewski & Goździewski 2009a) that the averaged 3D model may involve strongly chaotic motions, in the secular time-scale. To study in details, how the model parameters influence the structure of the  $\mathcal{S}$ -plane, and how it relates to the long-term chaotic phenomena, we apply the fast indicator approach. Among many numerical tools of this kind, we choose the so called *coefficient of the diffusion of fundamental frequencies*  $\sigma$  introduced by (Laskar 1990). To check whether a phase space trajectory of a quasi-integrable Hamiltonian

system is regular (quasi-periodic) or irregular (chaotic), one integrates the equations of motion over two subsequent intervals of time, e.g.,  $[0, T]$  and  $[T, 2T]$ . Next, we resolve the frequencies in the discrete orbital signal with the help of refined FFT analysis (Laskar 1990), obtaining two estimates of a given frequency, say  $f_T$  and  $f_{2T}$ , over these two intervals of time. The coefficient of the diffusion of the fundamental frequency is then defined through:

$$\sigma = \left\| \frac{f_T}{f_{2T}} - 1 \right\|.$$

Clearly, if the signal does not change over time,  $\sigma \sim 0$  and this means that the phase trajectory is quasi-periodic (stable). If  $\sigma$  is significantly different from 0, the trajectory is chaotic and regarded unstable. In our calculations, we used a variant of the frequency analysis developed by (Šidlichovský & Nesvorný 1996), which is called the Frequency Modified Fourier Transform (FMFT). We also used publicly available code of the FMFT algorithm, kindly provided by David Nesvorný on his personal web-page<sup>3</sup>.

Because the secular evolution is associated with  $\omega_i$  angles, we compute the  $\sigma$  coefficient on the basis of complex time-series  $\{G_i(t)\exp i\omega_i(t)\}, \dots, i = 1, 2$ , where  $i$  is the imaginary unit. In this signal, the osculating eccentricity and pericenter argument for each planet are canonical action-angle variables. Hence, resolving its Fourier components, we may determine the leading amplitudes (proper eccentricities) and the fundamental frequencies of pericenter angles.

Next, we did massive integrations of the secular equations of motion. The initial conditions were selected at the grid of  $200 \times 100$  data points of the  $\mathcal{P}_S$ -plane. At each point of the dynamical map, we integrated the secular trajectory over  $\sim 10^4$  secular periods with respect to the *smaller* frequency (typically, one of the fundamental frequencies is much larger than the other one). Having the computed phase trajectory, we then find an estimate  $\sigma$ , as well as the maximal eccentricities attained by both orbits during the integration time (the so called *max e* indicator) as well as the amplitude of variation of the mutual inclination  $\Delta i \equiv (\max i_{\text{mut}} - \min i_{\text{mut}})$  attained during the integration time. These geometrical characteristics are very useful to understand the source of instabilities indicated and detected by the diffusion coefficient  $\sigma$ .

Figures 4–6 illustrate the results derived for the same system that energy levels are shown in Fig. 2. Subsequent figures are for  $\mathcal{A} = 0.12, 0.16, 0.2$ , respectively (see Figs. 2b,c,e for the respective levels of  $\mathcal{H}_{\text{sec}}$ ). (We note, that for  $\mathcal{A} = 0.08$  the view of the phase space is basically very simple and the motions are regular everywhere). The right-hand panel of each figure is for  $\sigma$ . The dynamical character of the phase-space trajectories is color-coded: black color means quasi-regular evolution of the secular system ( $\sigma \sim 10^{-6} - 10^{-8}$ ), and yellow colour is for strongly chaotic motions ( $\sigma \geq 10^{-4}$ ). The  $\sigma$ -maps reveals that almost the whole phase space is filled up with regular motions, and chaos appears only in some small regions in the  $\mathcal{P}_S$ -plane. For a reference, the coordinates of equilibria IVa, IIIa, IIIb, IVb+ and 0 (the equilibrium at the origin) are marked with circles. Dotted circle is for Lyapunov stable solution IVa, crossed circles are for unstable solutions 0, IIIa and IIIb, respectively. Equilibrium IVb+ is linearly stable and is marked with open circle. Clearly, trajectories close to unstable equilibria IIIa and 0 are chaotic. Let us note that unstable equilibrium IIIa lies in a very narrow, chaotic zone too.

Besides dynamical maps for  $\sigma$ , Figs. 4–6 illustrate geometric

<sup>3</sup> <http://www.boulder.swri.edu/~davidn/>



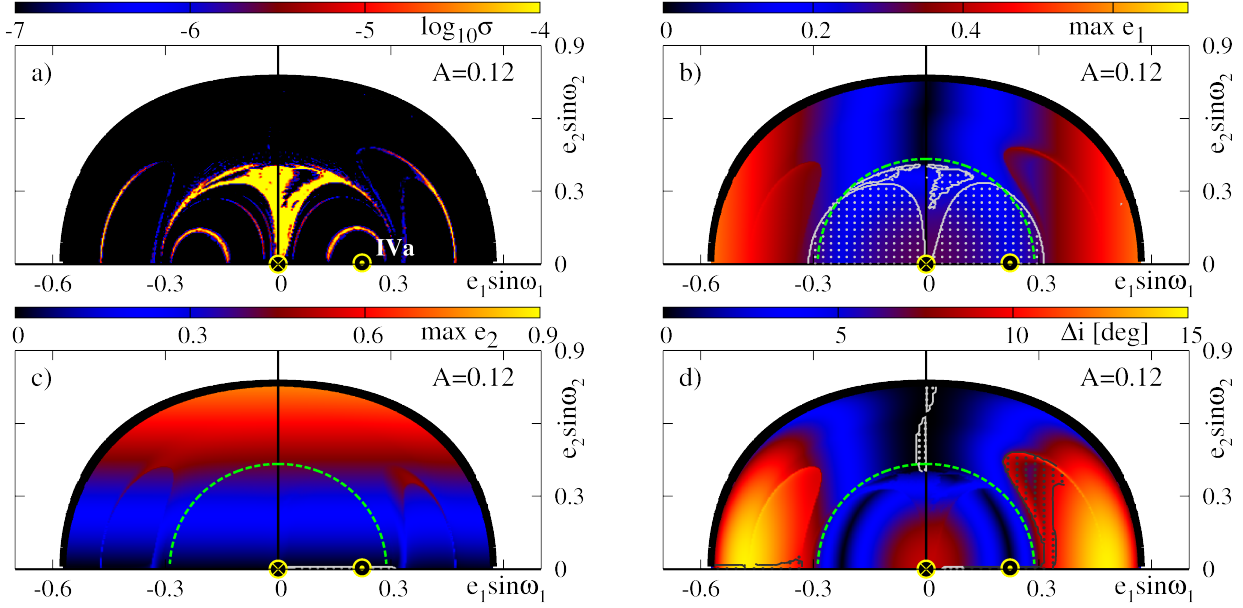


**Figure 4.** Dynamical maps for the classic (point-mass Newtonian) model, shown in the  $\mathcal{P}_3$ -plane. Panels from a) to d) are for the coefficient of the diffusion of fundamental frequencies ( $\sigma$ ), maximal eccentricity of the inner and outer planet ( $\max e_1, \max e_2$ ), respectively, and the amplitude of variation of the mutual inclination ( $\Delta i$ ). Dots mark areas of librations of  $\omega_1$  (panel b),  $\omega_2$  (panel c), and  $\Delta\omega$  (panel d). Stationary solutions are marked with circles: dotted circles are for stable equilibria (corresponding to the maximum of the secular Hamiltonian), crossed circles are for unstable equilibria, empty circles are for the linearly stable equilibria. These solutions are labeled, in accord with (Migaszewski & Goździewski 2009a). Parameters of the system:  $\alpha = 0.01, \mu = 20, \mathcal{A} = 0.12$ , see also Fig. 2b.

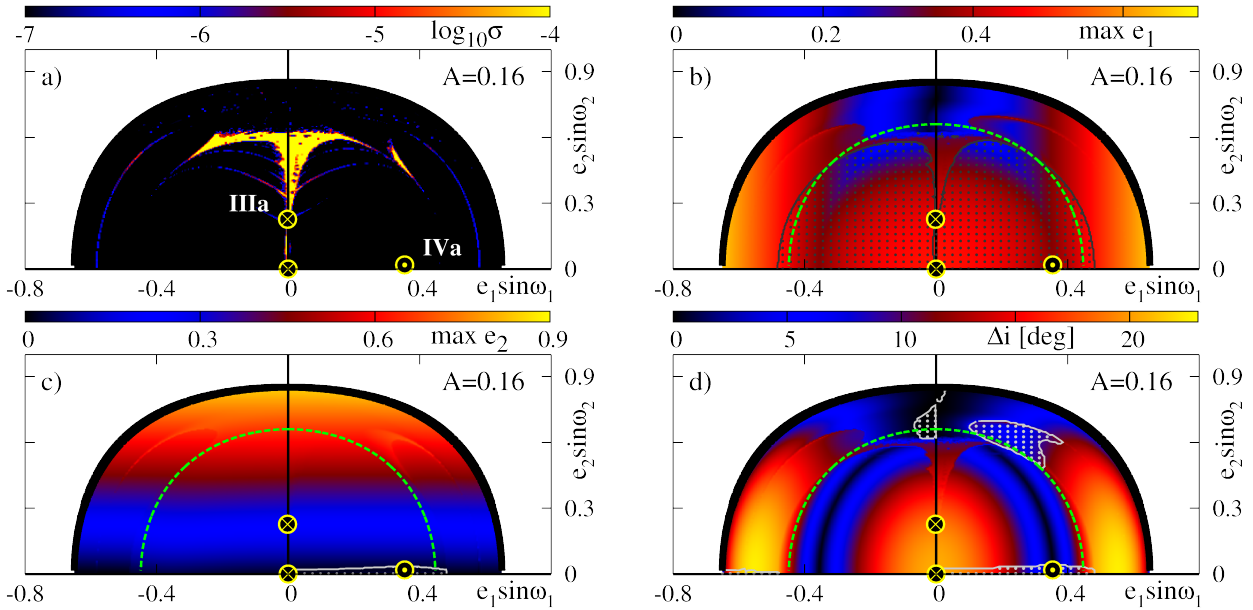


**Figure 5.** Dynamical maps for the Newtonian, point mass model in the  $\mathcal{P}_3$ -plane,  $\mathcal{A} = 0.16$ . See the caption to Fig. 4 for more details, and also Fig. 2c.

characteristics or orbits in the  $\mathcal{P}_3$ -plane, in terms of  $\max e_{1,2}$  indicator for the inner and the outer orbit, respectively, and for the amplitude of variation of the mutual inclination,  $\Delta i$ . In all these dynamical maps, the green dashed contours mark the mutual inclination equal to the critical inclination of the LKR bifurcation (Krasinski 1972, 1974). Also regions, in which the secular angles  $\omega_1$ ,  $\omega_2$ , and  $\Delta\omega$  oscillate, are shown: the gray/white/black dots surrounded by appropriate curves bound initial conditions that lead to librations of  $\omega_1$  around  $\pm\pi/2$  in the  $\max e_1$ -maps, librations of  $\omega_2$  around  $\pm\pi/2$

in the  $\max e_2$ -maps, and librations  $\Delta\omega$  around  $0, \pi$  in the  $\Delta i$ -maps. We note that  $\omega_1$  librates in almost all regular trajectories with the initial  $i_{\text{mut}} > i_{\text{crit}}$ . If this condition of the Lidov-Kozai mechanism is fulfilled then  $\omega_1$  librates around  $\pm\pi/2$ . In chaotic zones of the  $\mathcal{S}$ -plane, these angles do not oscillate, even if condition  $i_{\text{mut}} > i_{\text{crit}}$  holds true. Angle  $\omega_2$  librates around  $\pi/2$  only when  $e_2 \sim 0$ , for  $\mathcal{A} = 0.12, 0.16$ . This region extends significantly for larger  $\mathcal{A} = 0.2$ . In such a case, there are three zones in which *both* angles  $\omega_1$  and  $\omega_2$  librate: a region connected to equilibrium IVa, the neighborhood



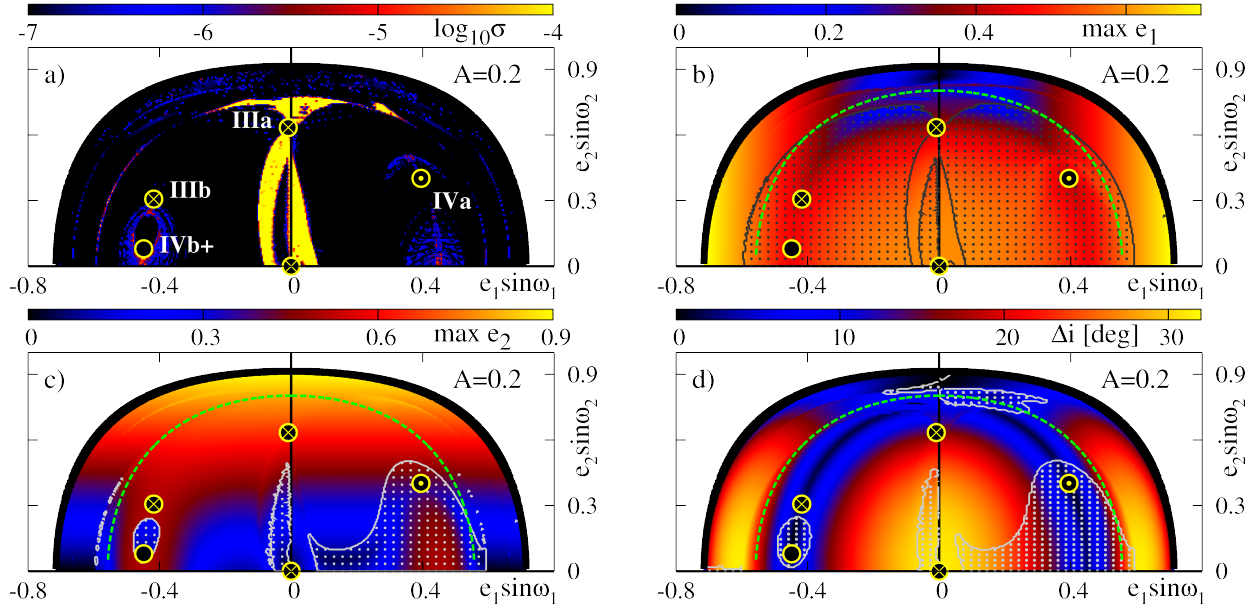


**Figure 6.** Dynamical maps for the Newtonian, point-mass model, in the  $\mathcal{P}_3$ -plane,  $\mathcal{A} = 0.20$ . See the caption to Fig. 4 for more details, also Fig. 2e.

of linearly stable solution IVb+, and a region of small  $e_1$  (though there is no stationary solution associated with these librations). The later area is surrounded by strongly chaotic motions shown in the  $\sigma$ -plane.

Clearly, the equilibria permitted by relatively large  $\mathcal{A}$  affect the secular dynamics, which become very complex. This may be better seen in the max  $e$ -maps. Subsequent panels in Figs. 4–6 show that the inner eccentricity may be strongly excited if  $i_{\text{mut}} > i_{\text{crit}}$ . For relatively small  $\mathcal{A} = 0.12$ , the inner orbit, which is initially quasi-circular, becomes moderately eccentric, with  $\max e_1 \sim 0.3$ . Note that in this specific case, the inner body is 20 times more massive than the outer companion. Simultaneously, as Fig. 4 shows, the outer eccentricity  $e_2$  is not amplified. We may conclude that in the regime of the outer LKR, when the inner body is much more massive than the outer body, the secular evolution may lead to strong perturbations of the inner orbit. Hence, even the mass hierarchy is reversed, a strong excitation of the inner eccentricity is still possible, similarly to the LKR in the restricted problem. This dynamical phenomenon may explain a large eccentricity of the binary, when a distant, low-mass and dark companion cannot be detected due to very long orbital period.

The dynamical maps in Figs. 4–6 reveal some zones, in which the outer eccentricity is strongly amplified. This eccentricity is obviously constant in terms of the quadrupole model. This feature of the octupole model shows that the small perturbation may cause extended, geometric changes of the mean orbits. The amplification of  $e_2$ , with simultaneously almost constant relative inclination,  $\Delta i \sim \text{const}$  (see Figs. 6c,d) seem appear due to the bifurcation of equilibria IVb+ and IIIb for  $\mathcal{A} \sim 0.195$ .

#### 4.1 A model explaining the secular chaos

The origin of chaotic secular dynamics may be explained by the presence of separatrices, which encompass different types of motions, librations and rotations of angles  $\omega_1$ ,  $\omega_2$  and  $\Delta\omega$ . A classification of these libration modes in the secular problem of two planets modes has been introduced in (Michtchenko et al. 2006). The

separatrices appear due to equilibria and periodic solutions in the integrable, or close to integrable secular models, which might be understood as the quadrupole approximation and/or the co-planar configuration.

Here, we found a simple explanation of the mechanism generating chaos, which is in fact the same as in the perturbed pendulum. To show this, let us recall that the expansion of  $\mathcal{H}_{\text{sec}}$  to the second order in  $\alpha$  is the celebrated integrable quadrupole-level model. The energy levels of this model are illustrated in Fig. 7a. Because  $e_2$  is the integral of motion, the representative plane may be constructed similarly to the integrable co-planar problem,  $S'' \equiv \{e_1 \cos 2\omega_1 \times e_2\}$ . In the region marked in green colour, any constant level of  $e_2$  crosses the energy curve in two turning points limiting the range of variation of  $e_1$ . If the  $e_2$  level is tangent to the given level of the energy, the dynamics must be then confined to fixed  $e_1$ , hence we obtain an equilibrium point (stable or unstable). A set of these equilibria for increasing, fixed values of  $e_2$  is marked by two thick curves that meet around of  $(e_1 = 0, e_2 \sim 0.4)$ . This is the bifurcation point, at which two families of equilibria emerge — the stable branch of the LKR and the unstable origin  $(e_1 = 0, e_2 = 0)$ .

For a given value of constant  $e_2$ , we may then find the maximum range of  $e_1$ , which corresponds to librations of the canonical angle  $\omega_1$ , and this value determines the position of separatrix, see Fig. 7b for the separatrix shown in the phase diagram in the  $\{e_1 \cos 2\omega_1 \times e_1 \sin 2\omega_1\}$ -plane, corresponding to the energy level marked by the blue curve on the levels diagram (Fig. 7a). Collecting such points along increasing  $e_2$ , we construct the red dashed curve in Fig. 7a, showing the separatrix region globally in the whole  $e_2$ -range (see the shaded area in Fig. 7a). The dashed line that marks the unstable origin, might be also understood as the other branch of the global separatrix, which, for any value of  $e_2$ , corresponds to the equilibrium point.

Now, considering the perturbed quadrupole-model in terms of the octupole-level secular expansion, we may expect that chaotic motions will appear close to the separatrix, due to the perturbation. Indeed, this is illustrated in two panels of Fig. 8. The left panel is for the frequency diffusion  $\sigma$  computed for initial conditions in the

$S'' \equiv \{e_1 \cos 2\omega_1 \times e_2\}$ -plane. This plane shows the energy levels of the octupole model, with stable (thick, solid curve) and unstable (thick, dashed line) equilibria in the quadrupole model overlotted. The red curve is for the global separatrix of the LK resonance in the quadrupole model, and the green region is for the librations of  $\omega_1$  in the integrable case. Clearly, chaotic orbits are found along the branch of unstable equilibria, as well as close to the red separatrix curve. This may be better seen in Poincaré cross section computed for a fixed energy level marked with blue curve that is shown in the right-hand panel of Fig. 8b. This panel in fact comprises *two* sections  $\Delta\varpi = \pi$  in the  $\{e_1 \cos 2\omega_1 \times e_1 \sin 2\omega_1\}$ -plane, for  $\Delta\varpi > 0$  (the left half-plane), and for  $\Delta\varpi < 0$  (the right half-plane). In place of the separatrix curves, a wide chaotic regions appear.

A careful inspection of Fig. 8a reveals additional narrow banana-shaped chaotic structures. They are related to the separatrix of the librations of angle  $\Delta\varpi$  around  $\pi$  and simultaneous circulation of angle  $\omega_1$ , which is classified as mode **2** in (Michtchenko et al. 2006, see their Fig. 3). Further, the plots of fundamental frequencies computed along the  $x$ -axis of the  $S'$ -plane in Fig. 8a, which are shown in Fig. 9, reveal that indeed, in this region the fundamental frequencies decrease to 0, indicating the separatrix region.

This example shows clearly that apparently very small perturbation (recall that  $\alpha = 0.01$ ) to the integrable model introduces extended chaotic behavior and qualitative change of the secular dynamics of the system.

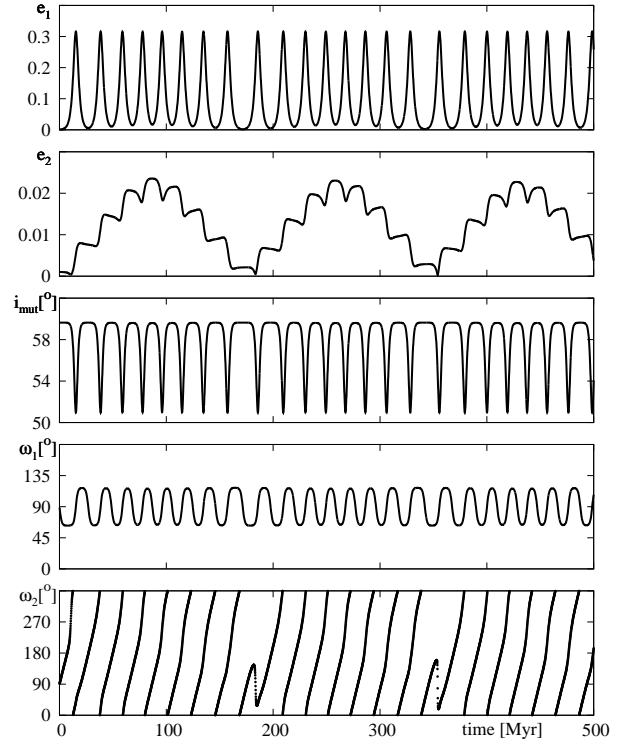
This interpretation is helpful to understand the source of chaotic motions shown in all dynamical maps (e.g., Figs. 4–6) – usually, they appear close to the separatrices associated with unstable equilibria or resonances of the secular angles (unstable periodic orbits).

Figure 10 shows the temporal evolution of the mean orbits with initial conditions close to the origin in Fig. 4 (see its caption for the details). The eccentricity of the inner orbit is significantly perturbed while the outer orbit is almost unchanged. The mutual inclination evolves in anti-phase with  $e_1$ , and  $\omega_1$  librates around  $\pi/2$ . These are typical features of the Lidov-Kozai resonance, still we recall that in this instance, the smaller outer body forces the LK cycles on the orbits of much more (20 times) massive than the inner component of the binary.

## 5 EQUILIBRIA IN THE CLASSIC OCTUPOLE MODEL

The dynamical maps and their analysis show that the equilibria constrain the secular dynamics of the perturbed model. In terms of the Newtonian, point-mass formulation, the stationary solutions depend on parameters  $\alpha$  and  $\mu$ . Limiting our survey to  $i_{\text{mut}} < \pi/2$  (direct orbits), we perform a parametric survey of the equilibria in terms of the octupole expansion, in such a manner that a comparison with the results derived for the more general, relativistic model will be possible. Here, we consider a more extended range of mass ratio  $\mu$ , covering a transition from the planetary regime (small  $\mu$ ) to the circumbinary case (large  $\mu$ ) than in (Migaszewski & Goździewski 2009a). Yet the assumption of small  $\alpha$  makes it possible to use the analytic formulation of the secular Hamiltonian, which is very precise in terms of the octupole-level approximation, instead of the numerical approach in (Migaszewski & Goździewski 2009a).

The parameter dependence of the equilibria is illustrated in Fig. 11 that shows the  $\mathcal{P}_S$ -plane (note that due to the symmetry, only the upper half-plane is illustrated, see also Fig. 3). We set  $\alpha = 0.04$ ,  $\mu \in [1.5, 3, 5, 10, 20, 25, 50]$ , and then positions of the equilibria may



**Figure 10.** The mean orbits with the following initial condition:  $m_0 = 1 m_\odot$ ,  $m_1 = 200 m_J$ ,  $m_2 = 10 m_J$ ,  $a_1 = 0.3$  au,  $a_2 = 30$  au,  $e_1 = 0.001$ ,  $e_2 = 0.001$ ,  $\omega_1 = \pi/2$ ,  $\omega_2 = \pi/2$ ,  $i_{\text{mut}} = 59^\circ.64$ ,  $\mathcal{A} = 0.12$ . Panels from the top to the bottom present the time-evolution of  $e_1, e_2, i_{\text{mut}}, \omega_1, \omega_2$ , respectively.

be traced along increasing  $\mathcal{A}$ , which might be understood as the natural curve parameter.

In fact, instead of  $\mu$ , we choose a new parameter  $\beta$  (see Krasinski 1974; Migaszewski & Goździewski 2010)

$$\beta(\mu, \alpha) \equiv L_1/L_2 \sim \mu\sqrt{\alpha},$$

that better reflects the dependence of the dynamics on *both*  $\mu$  and  $\alpha$  than on one of these parameters itself (we did a few numerical tests for different  $\alpha$  which confirm this scaling very well). Actions  $L_i$  reflect the angular momentum partition between both components. If  $\beta \sim 1$ , ( $\mu \sim 5$ ), both secondaries are dynamically equivalent, if  $\beta > 1$  ( $\mu > 5$ ) then the inner body “dominates” dynamically in the system, and if  $\beta < 1$  then the hierarchy is reversed. To illustrate the stability of the equilibria, the curves are marked with black dots are for Lyapunov stable solutions, and grey dots mean unstable solutions. The curves are labeled with both  $\mu$  and  $\beta$  parameters.

In the right-hand half-plane (quarter IV,  $\omega_1 = \omega_2 = \pi/2$ ), for  $i_{\text{mut}} < \pi/2$ , only one solution appears that is the LK resonance. For small  $\mu$ , it evolves with increasing  $\mathcal{A}$  along the axis of  $e_2 \sim 0$  between  $e_1 = 0$  (when the first LK bifurcation appears, see Fig. 2b) and  $e_1 \sim 1$ . After the second bifurcation of the LKR (Fig. 2e), two solutions emerge. One of them is the LKR for  $i_{\text{mut}} > \pi/2$  (see Migaszewski & Goździewski 2009a, this solution is not discussed here). The second new solution moves along the axis  $e_1 \sim 1$  up to large  $e_2$ .

For  $\mu \geq 2$ , the LKR does not reach  $e_1 = 1$  but it “turns back”, with decreasing  $e_1$  and increasing  $e_2$ . For larger mass ratio, the maximal  $e_1$  is smaller. The families of LKR for  $\mu = 1.5, 3$  correspond to systems with  $\beta < 1$ , hence the dynamical hierarchy is

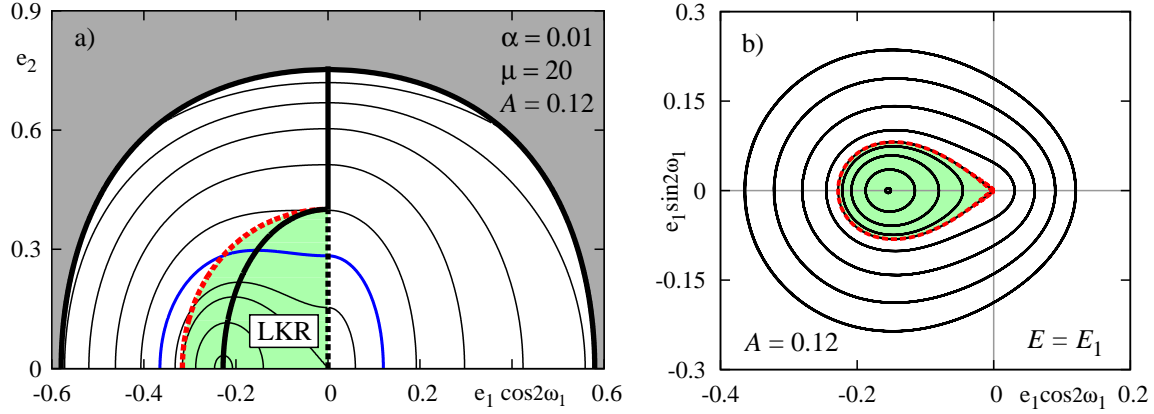


**Figure 7.** The left panel is for the levels of the secular energy (thin curves) depicted in the representative plane of the quadrupole problem,  $\mathcal{S}'' \equiv \{e_1 \cos 2\omega_1 \times e_2\}$ -plane,  $\alpha = 0.01$ ,  $\mu = 20$ ,  $\mathcal{A} = 0.12$ . Recall that this problem is integrable and  $e_2 \equiv \text{constant}$  is a parameter. The black, thick curve marks the LKR equilibrium for different energies and  $e_2$  integral. The red, dotted curve marks the separatrix between librations and rotations of  $\omega_1$  for fixed values of integrals. The shaded (green) zone indicates librations of  $\omega_1$  around  $\pi/2$ . The right hand panel is for the phase diagram in the  $\{e_1 \cos 2\omega_1 \times e_1 \sin 2\omega_1\}$ -plane and a fixed energy level marked by blue curve in panel a. The separatrix and the region of librations of  $\omega_1$  are also marked with green colour.

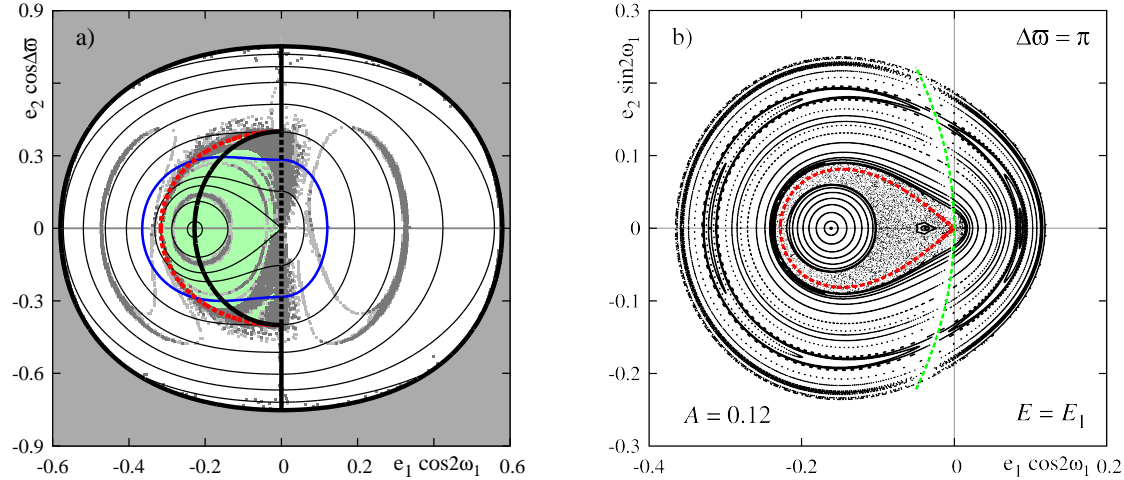


**Figure 8.** The left panel is for the secular energy levels (thin curves) shown in the  $\mathcal{S}'$ -plane of the octupole model,  $\alpha = 0.01$ ,  $\mu = 20$ ,  $\mathcal{A} = 0.12$ . Shaded areas are for initial conditions leading to chaotic evolution of the secular model. The red curve is for the separatrix of the LKR resonance in the quadrupole model, the black thick curve is for the equilibria in this model. The right hand panel is for the Poincaré cross-section  $\Delta\omega = \pi$  in the  $\{e_1 \cos 2\omega_1 \times e_1 \sin 2\omega_1\}$ -plane. It corresponds to a fixed energy level marked with the blue curve in panel a. The separatrix of the quadrupole problem and a region of librating  $\omega_1$  are also marked.

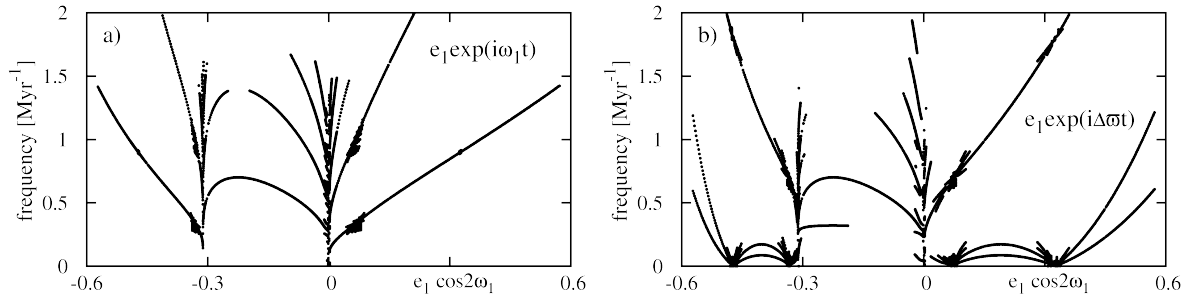


**Figure 9.** The spectrum of fundamental frequencies computed along the x-axis of Fig. 8, for the same set of parameters. Abscissas, in which the frequencies approach zero, indicate the separatrices of secular resonances of the respective angles,  $\omega_1$  (panel a), and  $\Delta\omega$  (panel b). Parameters are:  $m_0 = 1 m_\odot$ ,  $m_1 = 40 m_J$ ,  $m_2 = 2 m_J$ ,  $a_1 = 0.1 \text{ au}$ ,  $a_2 = 10 \text{ au}$ .

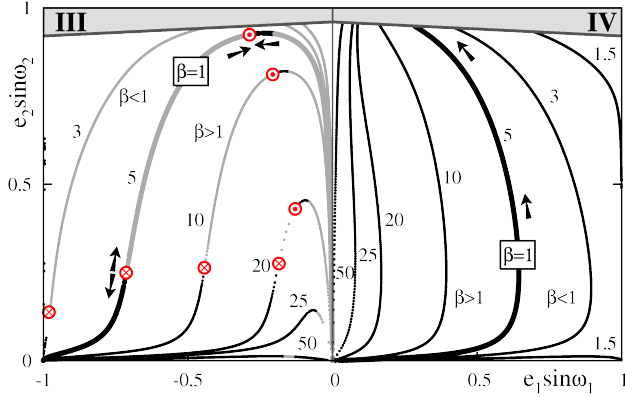


**Figure 11.** Families of stationary solutions in the  $\mathcal{P}_3$ -plane. The semi-major axes ratio  $\alpha = 0.04$ ,  $\mu = \{1.5, 3, 5, 10, 20, 25, 50\}$  (each curve is labeled accordingly with the value of  $\mu$ ). Dark dots are for stable equilibria, grey dots are for unstable equilibria. Crossed and dotted circles mark the positions on the equilibria curves where solutions bifurcate (see the text for details). Small arrows show the directions of the evolution of particular equilibrium with increasing  $\mathcal{A}$ . Parameter  $\beta \equiv L_1/L_2$  (see the text). Stationary curves corresponding to  $\beta = 1$  are drawn with thicker lines. Stationary solutions were calculated for the octupole classic model. See also Fig. 3.

reversed, and the eccentricity of the inner, *more massive* body is forced by the *outer* companion. The position of the LKR family moves to the region of smaller  $e_1$ , and for large enough  $\mu$ , this solution is confined to  $e_1 \sim 0$ -axis and tends to large  $e_2$ . The direction of parametric evolution of this equilibrium, corresponding to increasing  $\mathcal{A}$ , is marked with an arrow. We see that for all  $\mu$  this direction is the same.

The view of the left-hand half-plane is more complex. As we shown in (Migaszewski & Goździewski 2009a), the first solution appearing in quarter III of the  $\mathcal{P}_3$ -plane is unstable equilibrium IIIa emerging due to the second bifurcation of the origin ( $e_1 = e_2 = 0$ ) (marked with  $I_1^-$  in our paper). Then, with increasing  $\mathcal{A}$ , this solution moves along  $e_1 \sim 0$  towards large  $e_2$ . For some value of  $\mathcal{A}$  (e.g.,  $\sim 0.195$  for  $\alpha = 0.01$ ,  $\mu = 20$ ; see Fig. 3) solutions IIb and IVb+ appear in the same point of the phase space (this is illustrated with crossed circle in the left-hand half-plane of Fig. 3). Solution IVb+ then moves along  $e_1 \rightarrow 1$  and  $e_2 \rightarrow 0$ . Simultaneously, solution IIb evolves towards a point marked with dotted circle. Solution IIIa also moves to that point and for some critical  $\mathcal{A}$  both solutions merge and vanish. Figure 11 reveals that the parametric paths of equilibria depend on parameter  $\mu$  ( $\alpha = 0.04$  was fixed in this test). The path of the LKR becomes closer to  $e_1 \sim 0$ -axis for larger mass ratio. Also families of stationary solutions that are present in quarter III, become closer to the origin. The range of eccentricities corresponding to these equilibria is very small for  $\mu \geq 25$ . We may also notice that the bifurcation points (crossed and dotted circles, respectively) tend to each other with increasing mass ratio, which is consistent with the transition between the planetary and the circumbinary regime. For  $\mu \geq 25$ , these two points are merged. In this particular case, the structure of equilibria in quarter III of the  $\mathcal{P}_3$ -plane is more simple than in the general case because only one solution persists, a stable equilibrium corresponding to nearly circular outer orbit.

For different  $\alpha < 0.1$ , the general, global view of the families of equilibria is very similar to the results presented in Fig. 11. In fact, as we noticed previously, the parametric evolution of the

equilibria is reflected by parameter  $\beta(\mu, \alpha)$ , and basically does not depend on the individual values of  $\alpha$  and  $\mu$ .

## 6 THE PN CORRECTION TO THE SECULAR MODEL

The results presented in the previous section illustrate the already well known feature of the classic model (see, e.g., Michtchenko & Malhotra 2004; Michtchenko et al. 2006). In the approximation of small masses, the secular dynamics of the Newtonian 2-planet, hierarchical model depend on the semi-major axes ratio and planetary mass ratio, and not on individual system parameters,  $(a_1, a_2, m_1, m_2)$ . In our works (Migaszewski & Goździewski 2009b, 2010), we shown that this feature is not preserved in the more general model, including relativistic, rotational and tidal corrections to the Newtonian point-mass interactions. In these settings, the secular dynamics depend on the individual semi-major axes, as well as individual planetary masses. Because the overall structure of the phase space is characterized by the equilibria, we now attempt to show that deviations between these equilibria in the classic and relativistic models become more important when the system dimension scales down ( $a_1, a_2$  decrease when  $\alpha$  is const), and masses  $m_1, m_2$  are smaller, when their ratio  $\mu$  is kept constant.

The differences between the two coplanar models manifest itself through the shapes and localization of stationary solutions and depend on the *individual* masses and semi-major axes (Migaszewski & Goździewski 2009b). Now we can observe the same feature in the spatial planetary system, corrected for the relativistic perturbation. Figure 12 presents families of equilibria in the same manner as Fig. 11 (due to the symmetry, only the y-positive half-plane of  $\mathcal{P}_3$ -plane is presented). Families of stationary solutions in the classic model are drawn with blue and violet curves for stable and unstable solutions, respectively. Solutions in the relativistic model are plotted with black (stable equilibria) and grey (unstable equilibria) curves. In this experiment, we varied the individual masses of the secondary bodies, still keeping their ratio  $\mu = 10$  as a constant. The masses are changed between ( $m_1 = 100 m_j, m_2 = 10 m_j$ ) to ( $m_1 = 3 m_j, m_2 = 0.3 m_j$ ), and the primary mass is  $m_0 = 1 m_\odot$ .

The results illustrated in Fig. 12 confirm that even for large secondary masses, the parametric curves of stationary solutions in the realm of the classic model depends weakly on the individual masses. Yet similarly to the co-planar case, curves of equilibria calculated with the relativistic corrections differ significantly from the results obtained for the classic model. The deviations between both models are more significant for smaller masses of the secondary bodies. For instance, the family IVa moves to the range of much smaller  $e_1$ . Solutions of this type exist even for very small  $m_1$  and  $m_2$ , which is just not possible in the Newtonian model (Migaszewski & Goździewski 2009a). When the mutual perturbations between secondaries are small enough, the critical inclination in the relativistic model, that leads to the LK bifurcation, becomes larger than  $\pi/2$ . Thus  $i_{\text{crit}}$  increases with decreasing masses.

In quadrant III of the  $\mathcal{P}_3$ -plane ( $\omega_2 = -\omega_1 = \pm\pi/2$ ), the structure of equilibria is even more complex. For some critical values of masses ( $m_2 \sim 2.07 m_j$ ) the parametric paths divide into two parts. The top part, characterized by larger  $e_2$ , comprises of two unstable equilibria emerging from one bifurcation point, which then meet in another bifurcation point. The bottom part of the equilibria curve represents a saddle point, that changes its stability, from unstable IIIa-type solution to the stable solution IVb+. This branch is very similar to equilibria in the classic system with large  $\mu$  (or large

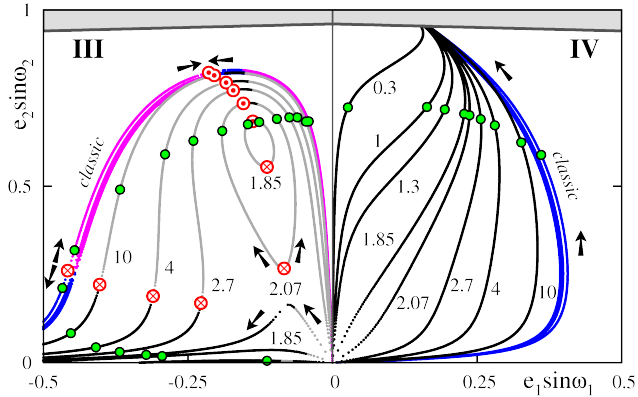


**Figure 12.** Families of stationary solutions presented in the  $\mathcal{P}_S$ -plane, calculated for  $\alpha = 0.04, \mu = 10, a_1 = 0.2 \text{ au}, a_2 = 5.0 \text{ au}, m_0 = 1 m_\odot$  and varied  $m_2 = 10, 4, 2.7, 2.07, 1.85, 1.3, 1.0, 0.3 m_J$ . Equilibria in the classic model are compared with the equilibria in the relativistic model. The mass of the outer body  $m_2$  labels each particular curve. Black dots are for stable equilibria, grey dots are for unstable equilibria of the relativistic model. Equilibria of the classic model are plotted with blue and violet dots for stable and unstable solutions, respectively. Positions of equilibria were calculated with the help of the octupole theory.

$\beta > 5$ ) observed already in Fig. 11, however this takes place for quite a different value of  $\beta = 2$ .

The stationary solutions are determined by the shape of the secular Hamiltonian. Its levels are plotted in the  $\mathcal{P}_S$ -plane, Fig. 13. Each panel in this figure is calculated for the same parameters  $\mu, \alpha, \mathcal{A}$  (but in this case, particular values of masses and semi-major axes are varied). Let us recall, that Fig. 13a shows the phase space calculated in classic model, while subsequent panels 13b,c,d are for relativistic model, and different masses and semi-major axes, labeled in subsequent panels.

If the masses are large (Fig. 13b), we can see four elliptic points separated by four saddles (let us recall that the  $\mathcal{P}_S$ -plane is redundant, and the energy levels are reflected with respect to the origin, thus in fact we have only two unique elliptic points and only two saddles). The elliptic points may be identified with solutions IVa ( $\omega_1 = \omega_2 = \pm\pi/2$ ) and IIb ( $\omega_1 = -\omega_2 = \pm\pi/2$ ). The saddles correspond to solutions IIIa ( $e_1 \sim 0$ ) and IVb+ ( $e_2 \sim 0$ ). When the masses decrease (still,  $\mu$  is kept constant), the structure surrounding solution IIb becomes smaller and moves towards solution IIIa. Simultaneously, the saddle point IVb+ tends to the origin. For the masses small enough, (Fig. 12), solutions IIIa and IIb merge and vanish, while IVb+ “falls” into the origin.

Figures 14–16 shows the dynamical maps for the relativistic model, and are constructed in the same manner as maps in Figs. 4–6. Subsequent figures correspond to masses and  $\mathcal{A}$  used to plot the energy levels in Figs. 13a,c,d respectively: Fig. 14 is for classic model, Figs. 15 and 16 are for the relativistic model with  $m_2 = 10 m_J$  and  $m_2 = 1.85 m_J$ , respectively. The mass ratio is  $\mu = 10$  in both instances. The order of panels and symbol-coding of equilibria, as well as coding libration zones of the angles  $\omega_1, \omega_2$ , and  $\Delta\omega$  are the same as in Figs. 4–6; in particular, dotted, crossed and empty circles mark the Lyapunov stable, unstable and linearly stable equilibria, respectively. Clearly, the overall view of the phase space is different in all cases. The regions of chaotic motions (yellow areas in the  $\sigma$ -maps) obtained for the classic and relativistic model are significantly different. Also the dependence on the masses of secondaries in the relativistic models is evident.

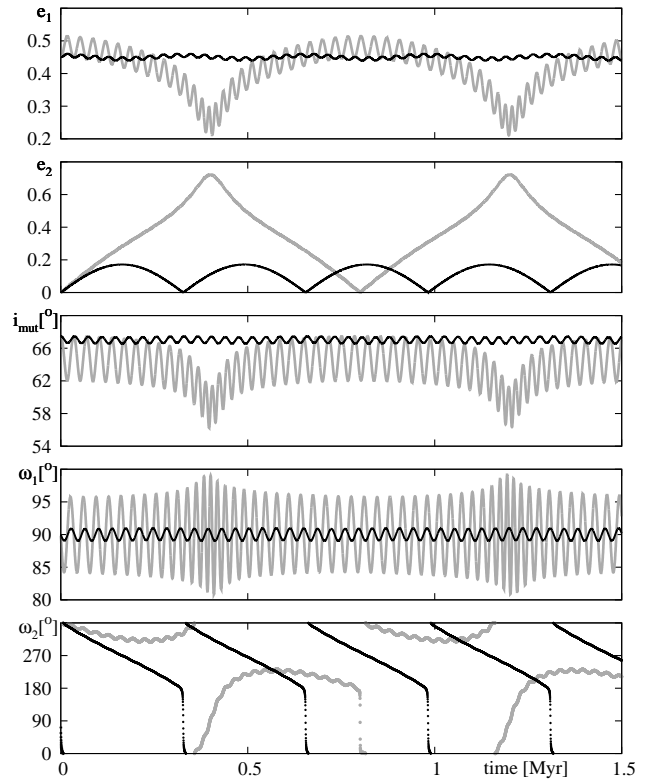
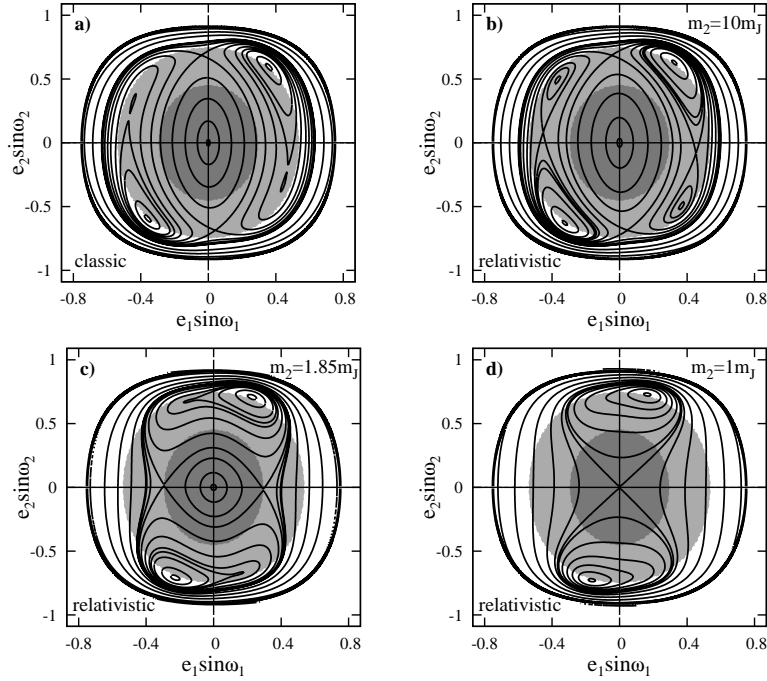


**Figure 17.** Evolution of the mean orbits in the following system:  $m_0 = 1 m_\odot, m_1 = 100 m_J, m_2 = 10 m_J, a_1 = 0.2 \text{ au}, a_2 = 5 \text{ au}, e_1 = 0.45, e_2 = 0.001, \omega_1 = \pi/2, \omega_2 = \pi/2, i_{\text{mut}} = 67.46^\circ, \mathcal{A} = 0.215$ . Panels from the top to the bottom illustrate the evolution of  $e_1, e_2, i_{\text{mut}}, \omega_1, \omega_2$ , respectively. The grey curves are for the classic secular model, the black curves are for the model including the relativistic corrections to the potential of the inner binary.

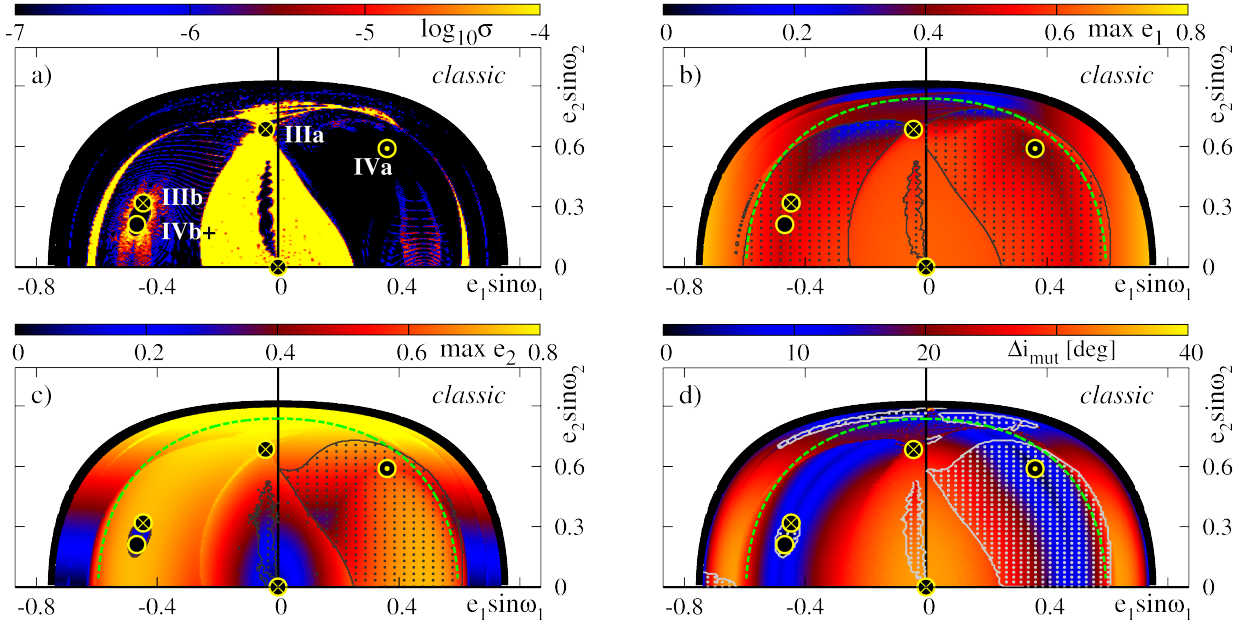
The structure of chaotic/regular secular evolution is reflected in max  $e_{1,2}$ -maps and through librational regions of  $\omega_1$  and  $\omega_2$ . We note, that in the case of the regular solutions,  $\omega_1$  librates around  $\pm\pi/2$  when  $i_{\text{mut}} > i_{\text{crit}}$ . In some part of this region also  $\omega_2$  librates around  $\pm\pi/2$ .

Figure 17 illustrates the temporal evolution for an initial condition written in the caption. The parameters of this model are the same as in Fig. 14. We chose the same initial eccentricities  $e_1 = 0.45$  and  $e_2 = 0.001$ , and integrate the secular equations of motion of classic (grey curves) and relativistic (black curves) models. We note qualitative differences between both configurations. The classic model leads to much larger variations of the elements. Particularly, the outer eccentricity  $e_2$  is strongly amplified, compared to the variations in the relativistic model. Still, this is not a rule. Inspecting the bottom row of Fig. 16, we can find regions in the  $\mathcal{P}_S$ -plane, in which, for the same initial condition, max  $e_2$  becomes larger in the relativistic model than in the Newtonian model. Also the secularly chaotic configurations appear in quite different zones of the phase space in both models. Moreover, the relativistic corrections may transform the regular evolution in the classic model into the chaotic evolution in the relativistic systems, and *vice versa*. Remarkably, the configuration illustrated in Fig. 14 has very large masses  $m_1 = 100 m_J$  and  $m_2 = 10 m_J$ .





**Figure 13.** Energy levels presented in the  $\mathcal{P}_5$ -plane, and calculated for the following parameters  $\alpha = 0.04, \mu = 10, \mathcal{A} = 0.215, i_0 = 84^\circ, a_1 = 0.2 \text{ au}, a_2 = 5.0 \text{ au}, m_0 = 1 m_\odot$ . A sequence of panels demonstrates the view of the phase space when masses of the secondary bodies decrease (their ratio is constant). From panel b) to panel d)  $(m_1, m_2)[m_j]$  are  $(100, 10), (18.5, 1.85), (10, 1)$ . Shaded areas mark ranges of  $i_{\text{mut}}$  larger than  $60^\circ, 75^\circ$ , (the light- and dark- grey, respectively).



**Figure 14.** Dynamical maps for the classic, Newtonian model in the  $\mathcal{P}_5$ -plane. The model parameters are  $\alpha = 0.04, \mu = 10, \mathcal{A} = 0.215, i_0 = 84^\circ, a_1 = 0.2 \text{ au}, a_2 = 5.0 \text{ au}, m_0 = 1 m_\odot, m_1 = 100 m_j, m_2 = 10 m_j$ . See the text and caption to Fig. 4 for the details.

## 7 CONCLUSIONS

In this work, we attempt to show that the global features of the secular dynamics of spatial, non-resonant planetary system depends qualitatively on the apparently subtle relativistic corrections to the Newtonian gravity. A lesson which we learned studying the coplanar case (Migaszewski & Goździewski 2009b) is that the *non-*

*Newtonian point-mass interactions* might be very important for the global dynamics of the system, because, in contrary to intuition one may have, the corrections to the Newtonian interactions might be *not small*, compared to the mutual point-to-point gravity. The numerical analysis of this multi-parameter problem is complex, hence the underlining idea of this paper lies in a construction of possi-



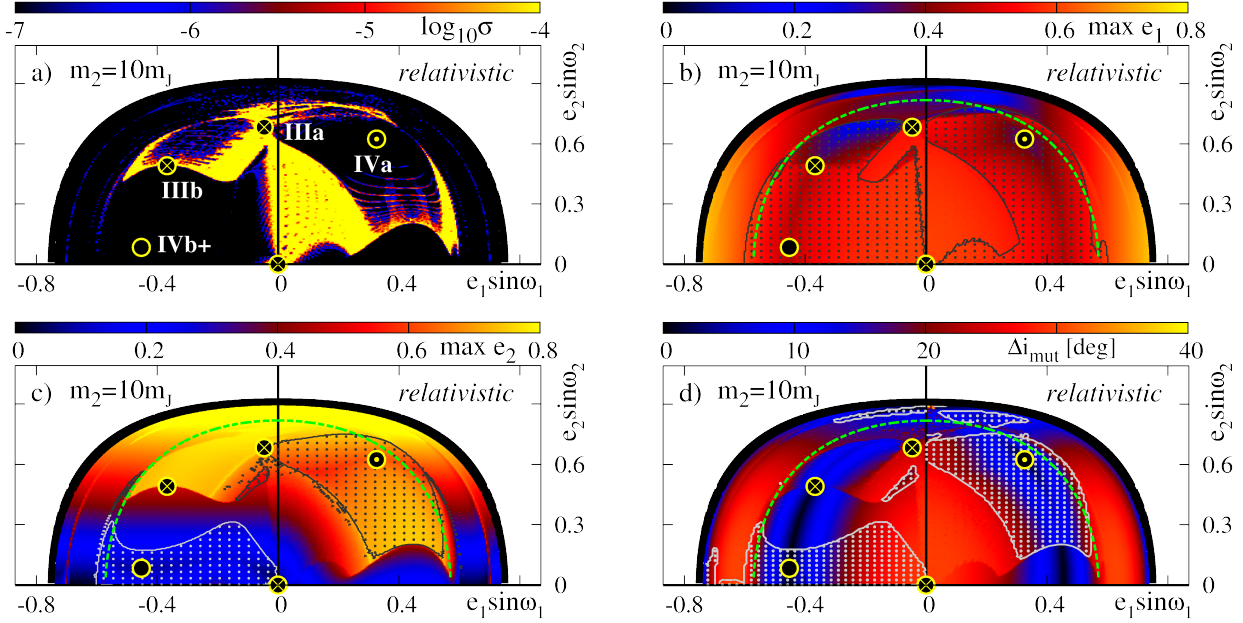


**Figure 15.** The dynamical maps for the octupole model with relativistic corrections. Masses of the secondary bodies are  $m_1 = 100m_J$ ,  $m_2 = 10m_J$ . See the text and caption to Fig. 4 for more details.

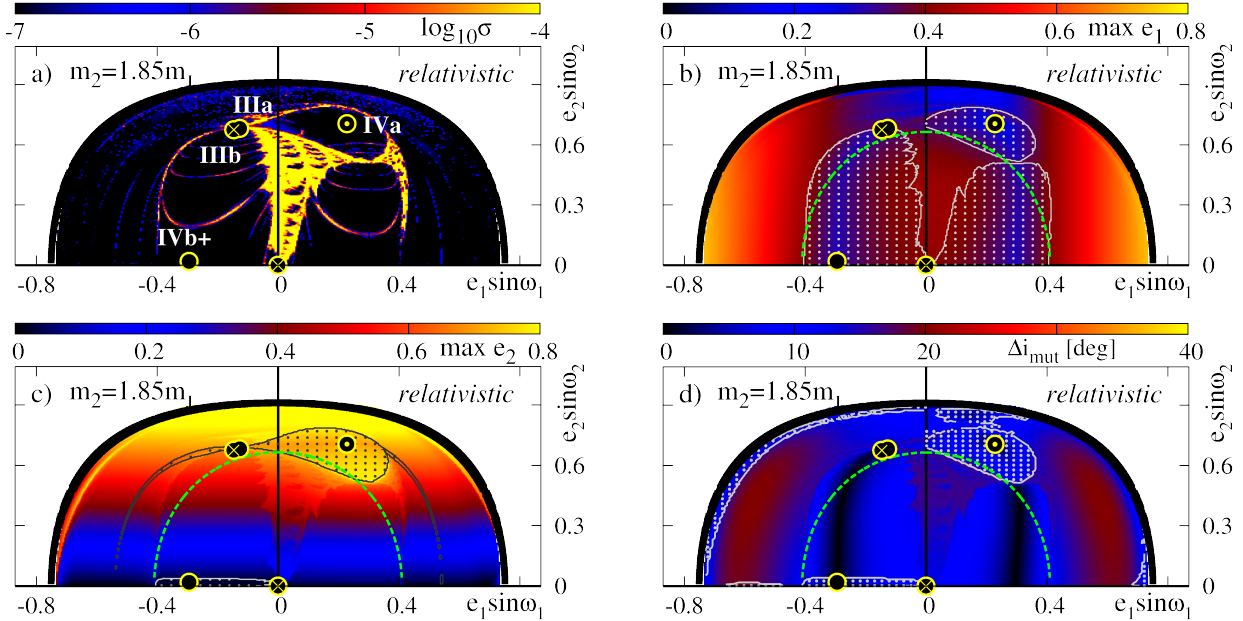


**Figure 16.** The dynamical maps for the octupole model with relativistic corrections. Masses of the secondary bodies are  $m_1 = 18.5m_J$ ,  $m_2 = 1.85m_J$ . See the text and caption to Fig. 4 for more details.

bly precise analytical model. A basically simple averaging of the perturbing Hamiltonian in (Migaszewski & Goździewski 2008), makes it possible to derive the analytic secular theory up to the order of 10 in the semi-major axes ratio  $\alpha$ . The accuracy of this model may be compared with the results of the numerical averaging of the perturbation (Michtchenko & Malhotra 2004). For a class of hierarchical systems considered in our paper, already the third-order model is precise enough to find and investigate the qualitative features of the system. In this work, we focus on three-body configurations, e.g., a star and two planets or a binary stars and one

planet. “Fortunately”, the second-order model is integrable, hence the octupole-level approximation might be considered as the first order perturbation to this integrable case. This makes it possible to understand the sources of instabilities appearing in the full system.

The averaging over mean anomalies reduces the dynamics to a system having two DOF, which then may be investigated with the help of rich geometrical tools, like the Poincaré cross section and the representative planes of initial conditions introduced in Michtchenko et al. (2006). Unfortunately, all additional corrections that increase the DOF number must be neglected here, as for in-

stance the quadrupole moment of the star and/or of the planets. This is the price that must be paid for the possibly global model of the dynamics. In the assumed range of  $a_1$ , the relativistic “corrections” in fact compare with the Newtonian point-mass mutual interactions, and are much larger than other perturbations, like the tidal and rotational distortions of the bodies. These assumptions justify that the model takes into account the PN corrections only to the potential of star and the inner secondary.

Having the two DOF model, we investigate the simplest class of solutions that are the equilibria. We focus on the Lidov-Kozai resonance (LKR) in systems characterized by large range of the mass ratio  $\mu$ . This part extends the results derived for small  $\mu$  in (Migaszewski & Goździewski 2009a). We found that even much smaller outer body (planetary mass  $m_2$  with respect to sub-stellar values of  $m_1$ ) moving in a wide, highly inclined ( $i_{\text{mut}} > \sim 60^\circ$ ) orbit may significantly perturb the inner orbit. In turn, the restricted model of the circumbinary planet, when we assume that the planet does not influence the binary, is not generally valid, even if the inner mass  $m_1$  is 100 times larger than the outer body  $m_2$ .

We also studied the parametric structure of families of particular equilibria classified as IVa, IIIa, IIIb, IVb+ in (Migaszewski & Goździewski 2009a) for small  $\alpha$ . Thanks to this assumption, the analytic model makes it possible to investigate the transition between the planetary regime (small  $\mu$ ) and the circumbinary regime ( $\mu \sim 50, 100$ ). This study shows that solutions in the planetary problem may disappear for large mass ratio.

A particularly interesting feature of the ocupole model is the appearance of the *secular chaos*. We found that if  $i_{\text{mut}}$  exceeds the critical inclination  $i_{\text{crit}}(\mu, \alpha)$ , the long term evolution of the system may be strongly chaotic, leading to large amplification of the eccentricities. In the regular regions of the phase space, the mean angle  $\omega_1$  librates around  $\pm\pi/2$ . In some parts of these regions also the second secular angle  $\omega_2$  librates around  $\pm\pi/2$ . The initial conditions satisfying  $i_{\text{mut}} > i_{\text{crit}}$  lead to strong amplification of the inner eccentricity  $e_1$ . Simultaneously, for the same values of the angular momentum of the system, we may observe strong amplification of  $e_2$  in some region of the phase space, with almost *constant* relative inclination of the orbits. This behaviour may be attributed to unstable equilibrium IIIb emerging in the secular system. The amplification of  $e_1$  happens not only for librations of  $\omega_1$  around  $\pm\pi/2$  (in the LK regime), but also and particularly when this angle behaves chaotically, varying in the whole range of  $[0, 2\pi]$ . The dynamical maps reveal that the primarily source of the chaotic motions are the unstable equilibria and unstable periodic orbits in the full system, following the appearance of separatrices in the integrable, quadrupole-level model.

Thanks to the simple analytic model, the influence of relativistic correction  $\mathcal{H}_{\text{GR}}$  on the global secular dynamics of the problem might be clearly demonstrated. A simple proof of this influence is provided by the analysis of the equilibria in the perturbed model. The differences between the Newtonian and relativistic models are larger when the mutual interactions between the secondaries are weaker, e.g., when companion masses are smaller. Yet the dynamics are basically very simple up to the limit of the critical inclination, when the first bifurcation of the origin ( $e_1 = e_2 = 0$ ) occurs, and this feature of the dynamics is preserved in both models.

Our approach may be generalized for other perturbations, like the rotational and conservative tidal distortion of the bodies in the system. Unfortunately, in this case, the dimension of the hierarchical system cannot be generally reduced to two DOF. Moreover, these perturbations lead to even more interesting and intriguing dynamics, which we investigated in the co-planar case (Migaszewski

& Goździewski 2009b), and we work on a global approach suitable for the 3D systems.

## ACKNOWLEDGEMENTS

This work is supported by the Polish Ministry of Sciences and Education, Grants No. 1P03D-021-29 and 92/N-ASTROSIM/2008/0.

## REFERENCES

- Adams F. C., Laughlin G., 2006, *International Journal of Modern Physics D*, 15, 2133
- Arnold V. I., Kozlov V. V., Neishtadt A. I., 1993, *Dynamical systems III*, Springer Verlag
- Brouwer D., Clemence G. M., 1961, *Methods of celestial mechanics*. New York: Academic Press, 1961
- Brumberg V., 2007, *Celestial Mechanics and Dynamical Astronomy*, 99, 245
- Eggenberger A., 2010, in K. Goździewski, A. Niedzielski, & J. Schneider ed., *EAS Publications Series Vol. 42*. pp 19–37
- Fabrycky D., Tremaine S., 2007, *ApJ*, 669, 1298
- Farago F., Laskar J., 2010, *MNRAS*, 401, 1189
- Ferraz-Mello S., ed. 2007, *Canonical Perturbation Theories - Degenerate Systems and Resonance Vol. 345 of Astrophysics and Space Science Library*
- Ferrer S., Osácar C., 1994, *Celestial Mechanics and Dynamical Astronomy*, 60, 187
- Ford E. B., Kozinsky B., Rasio F. A., 2000, *ApJ*, 535, 385
- Gronchi G. F., Milani A., 1998, *Celestial Mechanics and Dynamical Astronomy*, 71, 109
- Harrington R. S., 1968, *AJ*, 73, 190
- Kozai Y., 1962, *AJ*, 67, 579
- Krasinskii G. A., 1972, *Celestial Mechanics*, 6, 60
- Krasinskii G. A., 1974 Vol. 62 of *IAU Symposium*. pp 95–116
- Laskar J., 2000, *Phys. Rev. Lett.*, 84, 3240
- Laskar J., 1990, *Icarus*, 88, 266
- Laskar J., Robutel P., 1995, *Celestial Mechanics and Dynamical Astronomy*, 62, 193
- Lee M. H., Peale S. J., 2003, *ApJ*, 592, 1201
- Libert A.-S., Henrard J., 2007, *Icarus*, 191, 469
- Lidov M. L., 1962, *Planetary and Space Science*, 9, 719
- Lidov M. L., Ziglin S. L., 1976, *Celestial Mechanics*, 13, 471
- Michtchenko T. A., Ferraz-Mello S., Beaugé C., 2006, *Icarus*, 181, 555
- Michtchenko T. A., Malhotra R., 2004, *Icarus*, 168, 237
- Migaszewski C., Goździewski K., 2008, *MNRAS*, 388, 789
- Migaszewski C., Goździewski K., 2009a, *MNRAS*, 395, 1777
- Migaszewski C., Goździewski K., 2009b, *MNRAS*, 392, 2
- Migaszewski C., Goździewski K., 2010, in K. Goździewski, A. Niedzielski, & J. Schneider ed., *EAS Publications Series Vol. 42*, . pp 385–391
- Murray C. D., Dermott S. F., 2000, *Solar System Dynamics*. Cambridge Univ. Press
- Rabl G., Dvorak R., 1988, *A&A*, 191, 385
- Richardson D. L., Kelly T. J., 1988, *Celestial Mechanics*, 43, 193
- Takeda G., Kita R., Rasio F. A., 2009, in *IAU Symposium Vol. 253 of IAU Symposium*, . pp 181–187
- Tamuz O. e. a., 2008, *A&A*, 480, L33
- Šidlichovský M., Nesvorný D., 1996, *Celestial Mechanics and Dynamical Astronomy*, 65, 137